ANALYTICAL SOLUTION FOR SINGLE PHASE MICROTUBE HEAT TRANSFER INCLUDING AXIAL CONDUCTION AND VISCOUS DISSIPATION

A THESIS SUBMITTED TO
THE GRADUATE SCHOOL OF NATURAL AND APPLIED SCIENCES
OF
MIDDLE EAST TECHNICAL UNIVERSITY

BY

MURAT BARIŞIK

IN PARTIAL FULFILLMENT OF THE REQUIREMENTS
FOR
THE DEGREE OF MASTER OF SCIENCE
IN
MECHANICAL ENGINEERING

JULY 2008

Approval of the thesis:

ANALYTICAL SOLUTION FOR SINGLE PHASE MICROTUBE HEAT TRANSFER INCLUDING AXIAL CONDUCTION AND VISCOUS DISSIPATION

submitted by **MURAT BARIŞIK** in partial fulfillment of requirements for the degree of **Master of Science in Mechanical Engineering, Middle East Technical University** by,

Prof. Dr. Canan Özgen _____
Dean, Graduate School of **Natural and Applied Sciences**

Prof. Dr. Kemal İder _____
Head of Department, **Mechanical Engineering**

Assist. Prof. Dr. Almıla Güvenç Yazıcıoğlu
Supervisor, **Mechanical Engineering Dept., METU** _____

Prof. Dr. Sadık Kakaç
Co-Supervisor, **Mechanical Engineering Dept., TOBB-ETÜ**_____

Examining Committee Members:

Assist. Prof. Dr. Cüneyt Sert _____
Mechanical Engineering Dept., METU

Assist. Prof. Dr. Almıla Güvenç Yazıcıoğlu _____
Mechanical Engineering Dept., METU

Prof. Dr. Sadık Kakaç _____
Mechanical Engineering Dept., TOBB-ETÜ

Assist. Prof. Dr. Tuba Okutucu _____
Mechanical Engineering Dept., METU

Assist. Prof. Dr. Murat Kadri Aktaç _____
Mechanical Engineering Dept., TOBB-ETÜ

Date: _____

I hereby declare that all information in this document has been obtained and presented in accordance with academic rules and ethical conduct. I also declare that, as required by these rules and conduct, I have fully cited and referenced all material and results that are not original to this work.

Name, Last Name: Murat BARIŞIK

Signature:

ABSTRACT

ANALYTICAL SOLUTION FOR SINGLE PHASE MICROTUBE HEAT TRANSFER INCLUDING AXIAL CONDUCTION AND VISCOUS DISSIPATION

Barışık, Murat
M.S., Department of Mechanical Engineering
Supervisor: Assist. Prof. Dr. Almıla Güvenç Yazıcıoğlu
Co-Supervisor: Prof. Dr. Sadık Kakaç

July 2008, 84 Pages

Heat transfer of two-dimensional, hydrodynamically developed, thermally developing, single phase, laminar flow inside a microtube is studied analytically with constant wall temperature thermal boundary condition. The flow is assumed to be incompressible and thermo-physical properties of the fluid are assumed to be constant. Viscous dissipation and the axial conduction are included in the analysis. Rarefaction effect is imposed to the problem via velocity slip and temperature jump boundary conditions for the slip flow regime. The temperature distribution is determined by solving the energy equation together with the fully developed velocity profile. Analytical solutions are obtained for the temperature distribution and local and fully developed Nusselt number in terms of dimensionless parameters; Peclet number, Knudsen number, Brinkman number, and the parameter κ. The results are verified with the well-known ones from literature.

Keywords: Micropipe Heat Transfer, Slip Flow, Rarefaction Effect, Axial Conduction, Viscous Dissipation

ÖZ

MİKROTÜPLERDE TEK FAZLI AKIŞKANLARDA ISI TRANSFERİNİN EKSEN BOYUNCA ISI İLETİMİNİN VE SÜRTÜNME ISISININ DAHİL EDİLDİĞİ ANALİTİK ÇÖZÜMÜ

Barışık, Murat
Yüksek Lisans, Makine Mühendisliği Bölümü
Tez Yöneticisi: Assist. Prof. Dr. Almıla Güvenç Yazıcıoğlu
Ortak Tez Yöneticisi: Prof. Dr. Sadık Kakaç

Temmuz 2008, 84 Sayfa

Mikrotüplerdeki iki boyutlu, hidrodinamik olarak gelişmiş, ısıl olarak gelişmekte olan tek fazlı laminar akışın ısı transfer analizi sabit duvar sıcaklığı ısıl sınır koşulu için analitik olarak incelendi. Akışkan sıkıştırılamaz, sabit termofiziksel özellikli kabul edildi. Sürtünme ısınması ve eksen boyunca ısı iletimi çalışmaya dahil edildi. Seyrelme etkisi, kayma hızı ve sıcaklık atlaması sınır koşulları ile kaygan akış rejimi için çalışmaya eklendi. Sıcaklık dağılımı, enerji denleminin tam gelişmiş hız profili ile birlikte çözümü ile belirlendi. Sıcaklık dağılımı, bölgesel ve tam gelişmiş Nusselt sayısı için, Peclet, Knudsen, Brinkman sayıları ve boyutsuz κ parametresi cinsinden analitik sonuçlar elde edildi. Elde edilen sonuçlar literatürdeki bilinen sonuçlarla karşılaştırıldı.

Anahtar Kelimeler: Mikrokanallarda Isı Transferi, Kaygan Akış, Seyrelme Etkisi, Eksen Boyunca Isı İletimi, Sürtünme Isısı

in memory of Azize Kirpi…

ACKNOWLEDGEMENTS

I would like to thank to my supervisor, Assist. Prof. Almıla Güvenç Yazıcıoğlu, and to my co-supervisor Prof. Dr. Sadık Kakaç to bring this important topic into my attention. I am deeply grateful to my supervisor and co-supervisor for their guidance, inspiration, invaluable help, and contributions to my scientific point of view throughout my graduate study.

I wish to express my sincere appreciation to my friends; Gültekin Coşkun, Münir Ercan, Doğuhan Taşçı, Türker Çakmak, Ozan Köylüoğlu and Baran Çırpıcı for their support and motivation they provided me throughout my graduate study.

Finally, I express my deepest gratitude to my family, for their continuous encouragement.

TABLE OF CONTENTS

LIST OF TABLES

LIST OF FIGURES

NOMENCLATURE

A_1, A_2	coefficients in Eq. (4.12)
B_1, B_2	coefficients in Eq. (4.46)
Br	Brinkman number
c_p	constant pressure specific heat, J/kgK
C_1	coefficient in Eq. (4.21)
C_2	coefficient in Eq. (4.35)
D	tube diameter, m
F_m	tangential momentum accommodation coefficient
F_t	thermal accommodation coefficient
h	convective heat transfer coefficient, W/m^2K
k	thermal conductivity, W/mK
Kn	Knudsen number, λ / L
L	length, m
Nu	Nusselt number
P	pressure, kPa
Pe	Peclet number, $k/\rho C_p$
Pr	Prandtl number, ν/α
R	tube radius, m
r	radial coordinate
r^*	dimensionless radial coordinate
Re	Reynolds number, $u_m D/\nu$
T	fluid temperature, K
T_i	fluid temperature at inlet, K
T_w	wall temperature, K
u_s	slip velocity, m/s
u^*	dimensionless velocity

u	velocity in axial direction, m/s
v	velocity in radial (vertical) direction, m/s
x	axial coordinate
x^*	dimensionless axial coordinate, x/(R Pe)

Greek Symbols

α	thermal diffusivity, m^2/s
γ	specific heat ratio
λ	mean free path, m
λ_n	eigenvalue
μ	dynamic viscosity, kg/ms
κ	coefficients in Eq. (4.37)
ν	kinematic viscosity, m^2/s
ρ	density, kg/m^3
θ	angular direction
Θ	dimensionless temperature, $(T-T_w)/(T_i-T_w)$
η	dimensionless radial (vertical) coordinate, $\rho_s\, r/R$
ξ	dimensionless axial coordinate, $\rho_s^2(2-\rho_s^2)\, x/(R\, Pe)$
ξ^*	dimensionless axial coordinate, $\rho_s^2(2-\rho_s^2)\, x/(R)$

CHAPTER 1

INTRODUCTION

Interest in micro- and nanoscale heat transfer has been explosively increasing in accordance with the developments in MEMS and nanotechnology during the last two decades. The aim of cooling micro- and nanoscale devices is an important subject for most engineering applications. Cooling of devices having the dimensions of microns is a completely different problem than what is analyzed in the macro world. Investigation of the flow characteristics of micro- and nanoscale flows is still a key research area. The fluid flow inside a micro- or nanochannel is not fully understood.
One can understand some of the advantages of using micro- and nanoscale devices in heat transfer, starting from the single phase internal flow correlation for convective heat transfer;

$$h = \frac{Nu \cdot k}{D} \tag{1.1}$$

where h is the convection heat transfer coefficient, Nu is the Nusselt number, k is the thermal conductivity of the fluid and D is the hydraulic diameter of the channel or duct. In internal fully developed laminar flows, Nusselt number becomes a constant. For example, for the case of a constant wall temperature, Nu = 3.657 and for the case of a constant heat flux Nu = 4.364 [1]. As Reynolds number, Re, is proportional to hydraulic diameter, fluid flow in channels of small hydraulic diameter will predominantly be laminar. The above correlation therefore indicates that the heat transfer coefficient increases as channel diameter decreases. As a result of the hydraulic diameter being of the order of tens or hundreds of micrometers in

forced convection, heat transfer coefficient should be extremely high. However, the question is whether Nu is still the same for micro flows.

In macroscale fluid flow and heat transfer, continuum approach is the basis for most of the cases. However, continuum hypothesis is not applicable for most of the microscale fluid flow and heat transfer problems. While the ratio of the average distance traveled by the molecules without colliding with each other, the mean free path (λ), to the characteristic length of the flow (L) increases, the continuum approach fails to be valid, and the fluid modeling shifts from continuum model to molecular model. This ratio is known as Knudsen number,

$$Kn = \frac{\lambda}{\mathrm{L}} \tag{1.2}$$

Knudsen number determines the flow characteristics. Beşkök and Karniadakis [2] defined four different flow regimes based on the value of the Knudsen number. The flow is considered as continuum flow for small values of Kn (< 0.001), and the well known Navier-Stokes equations together with the no-slip and no-temperature jump boundary conditions are applicable for the flow field. For 0.001 < Kn < 0.1, flow is in slip-flow regime (slightly rarefied). For 0.1< Kn < 10 flow is in transition regime (moderately rarefied). Finally, the flow is considered as free-molecular flow for large values of Kn (>10) (highly rarefied); the tool for dealing with this type flow is kinetic theory of gases.

As can be understood from the above information, rarefaction is very important for micro and nanoscale fluid flows since it directly affects the condition of flow. No-slip velocity and no-temperature jump boundary conditions are not valid for a rarefied fluid flow at micro and nanoscale. The collision frequency of the fluid particles and the solid surface is not high enough to ensure the thermodynamic equilibrium between fluid particles and the solid surface. Therefore, the fluid particles adjacent to the solid surface no longer attain the velocity and the

temperature of the solid surface; they have a tangential velocity at the surface (slip-velocity) and a finite temperature difference at the solid surface (temperature-jump), which eliminate the classical macroscale conservation equations. Gad-el-Hak [3] discusses these concepts in detail.

For the slip flow regime (0.001 < Kn < 0.1), which is the main interest of this study, slip velocity and temperature jump boundary conditions are added into the governing equations to include non-continuum effects, such that macro flow conservation equations are still applicable. As explained through kinetic theory of gases, Gad-el-Hak [3] introduces slip velocity and temperature jump as follows,

$$u_s = -\frac{2 - F_m}{F_m}\lambda\left(\frac{du}{dr}\right)_{r=R} \tag{1.3}$$

$$T - T_s = -\frac{2 - F_t}{F_t}\frac{2\gamma}{\gamma + 1}\frac{\lambda}{Pr}\left(\frac{\partial T}{\partial r}\right)_{r=R} \tag{1.4}$$

Equation (1.3) is the slip velocity for the cylindrical coordinate system, where F_m is the momentum accommodation factor, which represents the fraction of the molecules undergoing diffuse reflection. For idealized smooth surfaces, F_m is equal to zero, which means specular reflection. For diffuse reflection, F_m is equal to one, which means that the tangential momentum is lost at the wall. The value of F_m depends on the gas, solid, surface finish, and surface contamination, and has been determined experimentally to vary between 0.5 and 1.0. For most of the gas-solid couples used in engineering applications, this parameter is close to unity [4]. Therefore for this study, F_m in Eq. (1.3) is also taken as unity.

Equation (1.4) is the temperature jump for the cylindrical coordinate system, where γ is the specific heat ratio, Pr is the Prandtl number of the fluid and F_t is the thermal accommodation factor, which represents the fraction of the molecules reflected diffusively by the wall and accommodated their energy to the wall temperature. Its

value also depends on the gas and solid, as well as surface roughness, gas temperature, gas pressure, and the temperature difference between solid surface and the gas. F_t has also been determined experimentally, and varies between 0 and 1.0. It can take any arbitrary value, unlike momentum accommodation factor [4].

Furthermore, for micro scale, two important effects, axial conduction and viscous dissipation, should also be considered carefully. Their influence will be more as a result of higher gradients in micro flow. Axial conduction, proportional to Re and the streamwise temperature gradient, will not be dominated by the convective term in the presence of micro flows when Re becomes of the order of one. It has high influence on heat transfer and Nu values especially for low Peclet numbers. Analogously, viscous dissipation, proportional to Brinkman number, defined as $Br = \mu \cdot u_m^2 / k \cdot \Delta T$, and the velocity gradient, will have a higher effect because of high velocity gradients and small wall to fluid temperature difference. Viscous dissipation effect will change by the condition of flow. If heating process is applied, viscous dissipation, which is higher near the wall surface as a result of the high velocity gradient, will increase the temperature of fluid. Then, the temperature difference between the fluid and the wall will decrease, which leads to a decrease in heat transfer. However for cooling processes it will increase the temperature difference, in turn increasing the heat transfer.

The objective of this study is to analytically solve the Graetz problem, which is hydrodynamically developed, thermally developing, constant wall temperature circular pipe flow, including axial conduction, viscous dissipation, and rarefaction effects for air flow. To include the rarefaction effect, the problem will be assumed to be in the slip flow regime; slip velocity and temperature jump boundary conditions will be used with conventional Navier Stokes equations. Axial conduction and viscous dissipation effects will be taken into account to see the increased influence on Nu because of the cases in micro flow besides ones in macro flow. Through this analysis, closed form solution for Nu as a function of Pe, Br and Kn will be obtained.

For this purpose, a wide range of literature will be investigated in Chapter 2 for studies considering Graetz problem extended with streamwise conduction, viscous heating or micro flow effects analytically or numerically. Chapter 3 presents formulation of problem. In Chapter 4, the analysis will be given for fully developed velocity and developing temperature profiles. The difficulty of solving non homogeneous second order partial differential equation of energy will be eliminated by using Kummers confluent hypergeometric function after superposition the temperature profile. Furthermore, non-orthogonal characteristic of eigenfunctions resulting from axial conduction effect will be transformed into orthogonal form by the help of Gram Schmidt orthogonalization procedure, details of which are presented in the appendix. In Chapter 5, the results will be presented and discussed for both fully developed and thermally developing macro and micro flow cases. A comparison of outcomes with well known studies from literature will be made to show the validity of the analytical procedure. Finally, in Chapter 6, the study will be summarized and concluded with recommendations for future studies.

.

CHAPTER 2

LITERATURE SURVEY

Thermal entrance region problem for circular tubes, which is known as the Graetz problem, was first investigated by Graetz [5], and later independently by Nusselt [6], analytically. The authors both worked on incompressible fluid flowing through a circular tube with constant physical properties, having hydrodynamically developed and thermally developing flow for constant wall temperature boundary condition different than the uniform temperature of the fluid at the entrance. The procedure includes separation of variables technique and solution of Sturm Liouville problem, which results in an infinite series expansion in terms of eigenvalues and eigenfunctions. Equation (2.1) gives the result of Graetz's solution from Kakac[7] as,

$$Nu_{x,T} = \frac{\sum_{n=0}^{\infty} G_n \exp\left(-2\lambda_n^2 x^*\right)}{2\sum_{n=0}^{\infty}(G_n/\lambda_n^2)\exp\left(-2\lambda_n^2 x^*\right)} \tag{2.1}$$

In this equation, λ_n are eigenvalues and $G_n = -\frac{C_n}{2}R_n'(1)$ where R_n are eigenfunctions, C_n are summation constants, and $R_n'(1)$ are the derivatives of eigenfunctions evaluated at r^*=1, where r^* is dimensionless radius as $r^*=r/R$.

The authors both analyzed the problem by using just three terms of the infinite series solution and evaluated the fully developed flow Nusselt number as 3.6567935, while neglecting viscous dissipation and axial conduction. As a result of this exclusion, the effects of Pe and Br on Nu could not be visualized.

For a circular duct, Kakac [7] gives a list of the first 11 eigenvalues and constants of the Graetz problem, as shown in Table 1. Higher order eigenvalues and eigenfunctions can be found from [8] and eigenfunctions of the Graetz problem solution for flat conduits can be found from [9].

Table 1 Eigenvalues and constants of the Graetz Problem

n	λ_n	C_n	G_n
0	2.70436	1.47643	0.74877
1	6.67903	-0.80612	0.54382
2	10.67337	0.58876	0.46286
3	14.67107	-0.47585	0.41541
4	18.66987	0.40502	0.38291
5	22.66914	-0.35575	0.35868
6	26.66866	0.31916	0.33962
7	30.66832	-0.29073	0.32406
8	34.66807	0.26789	0.31101
9	38.66788	-0.24906	0.29984
10	42.66773	0.23322	0.29012

Solution of the developing temperature distribution, Eq. (2.1) is a series solution converging uniformly for all nonzero values of x^*. However, the convergence is extremely slow as x^* approaches zero. Number of terms included in the summation affects convergence so critically that even using the first 121 terms of the series is not sufficient to find the local Nusselt number values for x^* less than 10^{-4} as explained by Shah [10]. Thus, the advantage of the thinness of the nonisothermal region of the very early part of entrance region can be used to develop a similarity

solution for this portion. Therefore, for x^* less than 10^{-4}, Leveque asymptotic solution [11] can be employed, which becomes increasingly accurate as x^* approaches to zero. The temperature distribution and the Nusselt number due to Leveque are given by

$$\theta = \frac{T_w - T}{T_w - T_e} = \frac{1}{\Gamma(\frac{4}{3})}\left(\int_0^{\mathrm{X}} e^{-\mathrm{X}^3} d\mathrm{X}\right) \tag{2.2}$$

Where

$$X = \frac{1 - (r/a)}{(9x^*)^{1/3}} \tag{2.3}$$

As a result,

$$Nu_{x,T} = \frac{2}{\Gamma(\frac{4}{3})(9x^*)^{1/3}} \tag{2.4}$$

In this approximation, temperature changes are confined to a region near the tube wall so that a new radial coordinate X, based on the wall, was used. As mentioned before, heat transfer is very close to the pipe wall so that the dimensionless penetration depth showing the effect of change in fluid temperature gets very low values. When considering axial position such that x^* is much less than 1, the fluid remains at the inlet temperature except near the wall. Therefore, dimensionless temperature θ varies from one (the wall temperature) to zero (the inlet temperature) as X varies from zero to dimensionless penetration depth, in this part of flow. Therefore, an order of magnitude analysis is used to determine the dominant terms in the energy equation and to understand how the thermal penetration depth grows along the tube. As a result, Leveque solution is valid only in a very restricted thermal entrance region where the depth of temperature penetration is of the same order of magnitude as the hydrodynamic boundary layer over which the velocity distribution may be considered linear.

Shah and London [10] reviewed the works done to improve the Graetz solution. Many researchers studied the effects of axial conduction, viscous dissipation, and rarefaction.

Including the axial conduction effect is an interesting problem due to the non-orthogonal characteristic of eigenfunctions. For macro flow, axial conduction is important for high Pe and for the early part of entrance region. Axial conduction is added into the Graetz problem, which means finding Nu as a function of Pe for hydrodynamically developed and thermally developing laminar pipe flow with constant wall temperature boundary condition. Many researchers [12-32] studied this problem for macro flow case. Some important works show the variation of Nu with Pe. For example, Ash and Heinbockel [25] enhanced the work of Pahor and Strand [26] by using confluent hypergeometric function to investigate fully developed flow. Shah and London [10] tabulated the fully developed Nu values of Ash and Heinbockel for different Pe values, as presented in table 2. Also, Michelsen [20] used the method of orthogonal collocation and obtained the same result as Ash (table 2). For thermally developing regime, Millsaps [31] solved the problem by using an infinite series of Bessel functions of zeroth order. The author gave the first four eigenvalues and eigenfunctions for Pe equal to 200 and 2000. Singh [30] also worked on the same problem as Millsaps. In addition to the first four eigenvalues and eigenfunctions, the author found the first six eigenvalues by an approximate method for Pe equals to 2, 10, 20, 100, 200, 2000 and ∞. Furthermore, Taitel [22] also presented the solution in a closed form by the integral method. The author used the second, third and fourth order polynomial approximations for the temperature profile and defined the Nu based on enthalpy change of the fluid from the entrance. For a numerical solution of Graetz problem, Schmidt [32] found the local Nu by using finite difference method. Hennecke [27] also used finite difference method to analyze the problem numerically and presented the results graphically for Pe equals to 1, 2, 5, 10, 20 and 50. Table 3 shows Nu values of Hennecke throughout the thermally developing region for different Pe values. For the early part of the developing region, Kader [28] used the Leveque method including axial conduction

into Graetz problem. The solution is applicable for dimensionless axial distance less than 0.06.

.

Table 2 Nu values for fully developed laminar flow in a pipe with constant wall temperature boundary condition for different Pe values

.

Pe	Nu	Pe	Nu	Pe	Nu	Pe	Nu	Pe	Nu	Pe	Nu
∞	3.6568	20	3.670	6	3.744	1	4.030	0.5	4.098	0.04	4.170
60	3.660	10	3.697	5	3.769	0.9	4.043	0.4	4.118	0.03	4.175
50	3.660	9	3.705	4	3.805	0.8	4.059	0.3	4.134	0.02	4.175
40	3.661	8	3.714	3	3.852	0.7	4.071	0.2	4.150	0.01	4.175
30	3.663	7	3.728	2	3.925	0.6	4.086	0.1	4.167	0.001	4.182

Table 3 Nu values for thermally developing laminar flow in a pipe with constant wall temperature boundary condition for different Pe values

x^*	$Nu_{x,T}$						
(x/(R Pe))	Pe=1	Pe=2	Pe=5	Pe=10	Pe=20	Pe=50	Pe=∞
0.005	-	-	-	-	34.0	18.7	12.82
0.001	-	-	-	46.2	21.6	13.6	10.13
0.002	-	-	50.7	24.5	13.4	9.6	8.04
0.003	-	-	35.1	17.3	10.8	8.0	7.04
0.004	-	68.9	27.4	13.8	9.0	7.1	6.43
0.005	-	55.0	21.9	11.3	7.8	6.5	6.00
0.01	65.0	30.0	12.2	7.1	5.6	5.1	4.92
0.02	32.9	15.8	7.1	5.0	4.4	4.2	4.17
0.03	22.9	11.4	5.5	4.3	4.0	3.9	3.89
0.04	17.4	9.2	4.9	4.0	3.8	3.8	3.77
0.05	14.4	7.8	4.5	3.9	3.72	3.71	3.71
0.1	8.5	5.3	3.9	3.70	3.67	3.66	3.66
0.2	5.5	4.3	3.77	3.70	3.67	3.66	3.66
0.3	4.7	4.0	3.77	3.70	3.67	3.66	3.66
0.4	4.5	3.92	3.77	3.70	3.67	3.66	3.66
0.5	4.3	3.92	3.77	3.70	3.67	3.66	3.66
1.0	4.03	3.92	3.77	3.70	3.67	3.66	3.66
2.0	4.03	3.92	3.77	3.70	3.67	3.66	3.66

The main conclusion of the abovementioned studies on the effect of axial conduction on Nu is that axial conduction is negligible for Pe>50. For Pe<50, axial conduction increases local and fully developed Nu and also the thermal entrance length.

Adding viscous dissipation effect into Graetz problem for the macro case is important for high velocity gas flows and moderate velocity viscous liquid flows. References [30, 33-35] worked on including viscous heating effect for the macro flow case. Brinkman [33] first investigated viscous dissipation effect and after him the viscous dissipation parameter Br was named. The author mainly worked on fluid temperature distribution for capillary flow in the presence of finite viscous dissipation by considering the duct wall temperature to be same as the fluid inlet temperature. By assuming small fluid temperature variations and constant viscosity, Brinkman found that the fluid temperature is highest near the tube wall as a result of highest rate of shear in this portion. To extend the Graetz solution with finite viscous dissipation, Ou and Cheng [34, 35] studied the problem with the boundary condition of constant duct wall temperature different from entering fluid temperature. The author used the eigenvalues method and found Nu showing the unique behavior of Br effect explained above. Furthermore, Singh [30] included both the axial conduction and viscous dissipation terms and tabulated the first four eigenvalues and eigenfunctions. As a result, the conclusion of researchers is that the viscous dissipation effect dominates the flow after some portion of entry region, which directly depends on the Brinkman number value.

The third important parameter to be included in Graetz solution is the rarefaction effect for micro flow. In light of the information given in the introduction section, the importance and advantages of the micro world can be understood. Sobhan and Garimella [36] summarized the studies on microchannel flows in the past decade and tabulated them. Some experimental results for microtubes and microchannels can be seen in Choi et al. [37] and Phafler et al. [38]. The difference between conventional models and microscale experiments shows the effect of Knudsen number. To understand the effect of microscale flow, Kavehpour et al. [39] used the slip flow model and their results showed an agreement with experimental results of Arkilic [40]. For high Kn values, the authors observed an increase in the entrance length and a decrease in Nusselt number.

Barron et al. [41] used the technique developed by Graetz to solve the problem of hydrodynamically developed, thermally developing circular tube flow extended to slip flow with constant wall temperature. Their solution procedure gives the first four eigenvalues with a good accuracy, but after the fifth root the method becomes unstable with unreliable eigenvalues. Furthermore, Barron et al. [42] found that over the slip flow regime, Nu was reduced about 40%. As a result of rarefaction, the maximum temperature decreases and the temperature profile becomes flat. Furthermore, increasing rarefaction causes an increase in the entrance length. For a micro flow, the fully developed condition is not obtained as quickly as in macro flow case. Change of entrance length with Kn can be shown with Eq. (2.5).

$$x_e = 0.0828 + 0.141Kn^{0.69} \tag{2.5}$$

Larrode et al. [43] solved the heat convection problem for gaseous flow in a circular tube in the slip flow regime with uniform temperature boundary condition. The effect of the rarefaction and surface accommodation coefficients were considered. The authors defined a new variable, the slip radius, $\rho_s^2 = \frac{1}{1+4\beta_v Kn}$, where β_v is a function of the momentum accommodation factor. As a result, they obtained the velocity profile like no slip velocity by scaling it with this new variable. Therefore, the velocity profile is converted to the one used for the continuum flow, $u = 1 - r^2$. The authors also defined a coefficient representing the relative importance of velocity slip and temperature jump as $\beta = \frac{\beta_T}{\beta_v}$, where $\beta_T = \frac{2-F_t}{F_t}\frac{2\gamma}{\gamma+1}\frac{1}{Pr}$, with γ being the gas constant and F_t the thermal accommodation coefficient. It was concluded that heat transfer decreases with increasing rarefaction in the presence of temperature jump due to the smaller temperature gradient at the wall. However it was noted that this was not true for all, since the eigenvalues are also dependent on the fluid-surface interaction. Depending on the values of the accommodation coefficients, Nu may also increase or stay constant with increasing Kn. For $\beta < 1$, Nu increases with increasing Kn since $\beta_v > \beta_T$ suggests increasing convection at the surface. However,

for $\beta > 1$, Nu decreases with increasing Kn due to the more effective temperature jump and thus reduced temperature gradient on the surface.

Mikhailov and Cotta have several works on eigenvalue problems [44, 45]. The authors [46] extended the Graetz solution by adding slip flow regime conditions and using Kummers hypergeometric function which is the most common type of confluent hypergeometric functions. The term confluent refers to the merging of two of the three regular singular points of the differential equation into an irregular singular point whereas the usual hypergeometric equation has three separate regular singular points. The Kummer's function can be obtained from the series expansion as Eq. (2.7) for the first kind confluent hypergeometric function solution of Eq. (2.6).

$$z\frac{d^2w}{dz^2} + (c - z)\frac{dw}{dz} - aw = 0 \tag{2.6}$$

$$1F1(a, c; z) = 1 + \frac{a \cdot z}{c} + \frac{a(a+1)}{c(c+1)}\frac{z^2}{2!} + \cdots = \sum_{n=0}^{\infty} \frac{a_n}{c_n}\frac{z^n}{n!} \tag{2.7}$$

where a_n and c_n are Pochhammer symbols. If a and c are integers, $a < 0$ and either $c > 0$ or $c < a$, then the series yields a polynomial with a finite number of terms. If c is an integer less than or equal to zero, then $1F1(a, c; z)$ is undefined. In addition to all, Bessel functions, error function, incomplete gamma function, and Hermite and Laguerre polynomials can be obtained from the Kummers function.

Additional to macro case reasons, viscous heat generation becomes more important in micro flows as mentioned in the introduction chapter. Researchers [47-51] added the effect of viscous dissipation for micro flow. Again including axial conduction effect is an interesting problem because of the non-orthogonal characteristic of eigenfunctions, but also it is more important for micro case. More recently, Barbaros et al [58] solved the Graetz problem with including axial conduction, viscous dissipation and rarefaction effects. Finite difference scheme was used to solve energy

equation and a good agreement with literature was obtained. Hadjiconstantinou and Simek [52] studied the effect of axial conduction for thermally fully developed flows in micro- and nanochannels. Jeong [53] worked on the extended Graetz problem considering streamwise conduction and viscous dissipation in microchannels with uniform heat flux boundary condition. He analyzed the energy equation by using eigenvalue expansion. He used numerical shooting method to obtain eigenvalues and eigenfunctions, which are non-orthogonal. Cotta et.al [54] added the axial conduction and viscous dissipation terms for slip flow regime of transient flow with isothermal boundary condition. The authors first applied the integral transform technique and then solved the remaining by using the abovementioned Kummers hypergeometric function. They included the integral transform of each component numerically using Method of Lines. Horiuchi et al. [55] studied the thermal characteristics of the mixed electroosmotic and pressure-driven flow with axial conduction analytically. Furthermore, Dutta [56] solved the energy equation of steady electroosmotic flow with an arbitrary pressure gradient for a two dimensional microchannel considering advective, diffusive, and Joule heating terms. He used an analytical solution for the second order differential problem and used Kummers hypergeometric functions to evaluate the non-orthogonal eigenfunctions. He used Gram Schmidt orthogonalization procedure to generate orthogonal eigenfunctions.

In this study, heat transfer for steady state thermally developing flow inside a microtube in the slip-flow regime is studied with constant wall temperature thermal boundary condition analytically. The effect of rarefaction, viscous dissipation, and axial conduction is included in the analysis. The energy equation is solved analytically by using confluent hypergeometric functions in order to provide a fundamental understanding of the effects of the non-dimensional parameters on the heat transfer characteristics. The orthogonal eigenfunctions are generated by Gram-Schmidt orthogonalization procedure. The closed form solution for temperature distribution and the Nusselt number are determined as a function of non-dimensional parameters.

CHAPTER 3

FORMULATION OF PROBLEM

Convective heat transfer is the study of heat transport processes between the layers of a fluid when the fluid is in motion and in contact with a boundary surface at a temperature different from the fluid. Governing equations for a cylindrical coordinate system for convective heat transfer of an incompressible Newtonian fluid having constant thermo-physical properties in the continuum regime are given below.

Continuity equation:

$$\frac{\partial u}{\partial x}+\frac{1}{r}\frac{\partial (rv)}{\partial r}+\frac{1}{r}\frac{\partial w}{\partial \theta}=0 \tag{3.1}$$

x-momentum equation:

$$\frac{\partial u}{\partial t}+u\frac{\partial u}{\partial x}+v\frac{\partial u}{\partial r}+\frac{w}{r}\frac{\partial u}{\partial \theta} = f_x-\frac{1}{\rho}\frac{\partial P}{\partial x}+\nu\left(\frac{\partial^2 u}{\partial x^2}+\frac{1}{r}\frac{\partial}{\partial r}\left(r\frac{\partial u}{\partial r}\right)+\frac{1}{r^2}\frac{\partial^2 u}{\partial \theta^2}\right) \tag{3.2}$$

r-momentum equation:

$$\frac{\partial v}{\partial t}+u\frac{\partial v}{\partial x}+v\frac{\partial v}{\partial r}+\frac{w}{r}\frac{\partial v}{\partial \theta}-\frac{w^2}{r} = f_r-\frac{1}{\rho}\frac{\partial P}{\partial r}+\nu\left(\frac{\partial^2 v}{\partial x^2}+\frac{\partial}{\partial r}\left(\frac{1}{r}\frac{\partial (rv)}{\partial r}\right)+\frac{1}{r^2}\frac{\partial^2 v}{\partial \theta^2}-\frac{2}{r^2}\frac{\partial w}{\partial \theta}\right) \tag{3.3}$$

θ-momentum equation:

$$\frac{\partial w}{\partial t}+u\frac{\partial w}{\partial x}+v\frac{\partial w}{\partial r}+\frac{w}{r}\frac{\partial w}{\partial \theta}+\frac{v\,w}{r} = f_\theta-\frac{1}{\rho r}\frac{\partial P}{\partial \theta}+\nu\left(\frac{\partial^2 w}{\partial x^2}+\frac{1}{r}\frac{\partial}{\partial r}\left(r\frac{\partial w}{\partial r}\right)+\frac{1}{r^2}\frac{\partial^2 w}{\partial \theta^2}+\frac{2}{r^2}\frac{\partial v}{\partial \theta}\right) \tag{3.4}$$

Energy equation:

$$\rho C_p\left(\frac{\partial T}{\partial t}+u\frac{\partial T}{\partial x}+v\frac{\partial T}{\partial r}+\frac{w}{r}\frac{\partial T}{\partial \theta}\right) = k\left(\frac{\partial^2 T}{\partial x^2}+\frac{1}{r}\frac{\partial}{\partial r}\left(r\frac{\partial T}{\partial r}\right)+\frac{1}{r^2}\frac{\partial^2 T}{\partial \theta^2}\right)+\mu\Phi \tag{3.5}$$

where,

$$\Phi = 2\left(\left(\frac{\partial u}{\partial x}\right)^2+\left(\frac{1}{r}\left(\frac{\partial w}{\partial \theta}+v\right)\right)^2+\left(\frac{\partial v}{\partial r}\right)^2\right)+\left(\frac{\partial v}{\partial x}+\frac{1}{r}\frac{\partial u}{\partial \theta}\right)^2+\left(\frac{\partial u}{\partial r}+\frac{\partial v}{\partial x}\right)^2+\left(\frac{1}{r}\frac{\partial v}{\partial \theta}+r\frac{\partial}{\partial r}\left(\frac{w}{r}\right)\right)^2 \tag{3.6}$$

and u, v, and w are the velocity components in x, r, and θ directions, respectively.

In our study, forced convective heat transfer analysis of two-dimensional, single phase, pressure driven, steady state, hydrodynamically developed, thermally developing laminar flow inside a microtube is studied with constant wall temperature thermal boundary condition. The flow is assumed to be incompressible and thermo-physical properties of the fluid are assumed to be constant. For the microscale case, the flow is considered to be in the slip flow regime such that continuum governing equations are still applicable with slip velocity (Eq. (1.3)) and temperature jump (Eq. (1.4)) boundary conditions. To obtain the fully developed velocity profile, it is assumed that there is an unheated portion of the micro tube. After this entrance region, the temperature distribution starts to develop. Geometry of problem is shown in Fig. 1.

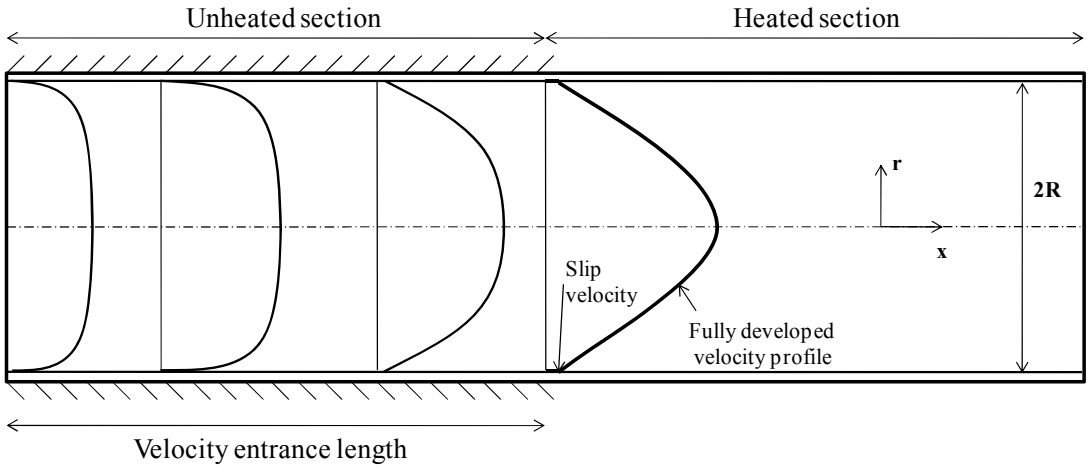

Figure 1 Geometry of problem

CHAPTER 4

SOLUTION METHOD

4.1. Fully developed velocity distribution:

For the flow conditions, steady state and two dimensional flow, the governing Eqs. (3.1), (3.2), and (3.3) can be written as Eqs. (4.1), (4.2), and (4.3) respectively.

Continuity equation:

$$\frac{1}{r}\frac{\partial(rv)}{\partial r}+\frac{\partial u}{\partial x}=0 \tag{4.1}$$

r-momentum:

$$u\frac{\partial v}{\partial x}+v\frac{\partial v}{\partial r}=-\frac{1}{\rho}\frac{\partial P}{\partial r}+\nu\left(\frac{\partial}{\partial r}\left(\frac{1}{r}\frac{\partial(rv)}{\partial r}\right)+\frac{\partial^2 v}{\partial x^2}\right) \tag{4.2}$$

x-momentum:

$$u\frac{\partial u}{\partial x}+v\frac{\partial u}{\partial r}=-\frac{1}{\rho}\frac{\partial P}{\partial x}+\nu\left(\frac{1}{r}\frac{\partial}{\partial r}\left(r\frac{\partial u}{\partial r}\right)+\frac{\partial^2 u}{\partial x^2}\right) \tag{4.3}$$

For steady and fully developed flow *u* is a function of *r* only and the velocity component *v* is zero everywhere. Therefore; continuity equation, Eq. (3.1) is satisfied identically and the Navier-Stokes Equations, Eqs. (4.2) and (4.3) reduce to Eqs. (4.4) and (4.5) respectively.

$$-\frac{1}{\rho}\frac{\partial P}{\partial r}=0 \tag{4.4}$$

$$-\frac{1}{\rho}\frac{\partial P}{\partial x}+\nu\left(\frac{1}{r}\frac{\partial}{\partial r}\left(r\frac{\partial u}{\partial r}\right)\right)=0 \tag{4.5}$$

From Eq. (4.4), it is concluded that the pressure, P must be constant across any section perpendicular to flow. Hence, Eq. (4.4) and (4.5) can be written as;

$$P=f(x) \tag{4.6}$$

$$\frac{dP}{dx}=\mu\left(\frac{1}{r}\frac{\partial}{\partial r}\left(r\frac{\partial u}{\partial r}\right)\right) \tag{4.7}$$

Since the left hand side of the Eq. (4.7) is a function of x only and the right hand side is a function of r only, the only possible solution is that both should be equal to a constant.

$$\frac{dP}{dx}=constant=-\frac{\Delta P}{L} \tag{4.8}$$

where ΔP is pressure drop over a length L of the tube. Hence, Eq. (4.7) becomes,

$$\frac{1}{r}\frac{\partial}{\partial r}\left(r\frac{\partial u}{\partial r}\right)=-\frac{\Delta P}{\mu L} \tag{4.9}$$

Integrating Eq. (4.9) twice yields,

$$\frac{\partial}{\partial r}\left(r\frac{\partial u}{\partial r}\right)=-\frac{\Delta P}{\mu L}r \tag{4.10}$$

$$\left(r\frac{\partial u}{\partial r}\right)=-\frac{1}{2}\frac{\Delta P}{\mu L}r^2+A_1 \tag{4.11}$$

$$u(r) = -\frac{1}{4}\frac{\Delta P}{\mu L}r^2 + A_1 lnr + A_2 \tag{4.12}$$

With boundary conditions,

$$r = 0, \qquad \frac{du}{dr} = 0 \tag{4.13}$$

$$r = R, \qquad u = u_s = -\lambda\left(\frac{du}{dr}\right)_{r=R} \tag{4.14}$$

where u_s is the slip velocity, which is defined as in Eq. (1.3), by taking F_m=1.
By applying the boundary conditions, A_1 and A_2 can be determined.

$$A_1 = 0 \tag{4.15}$$

$$A_2 = u_s - \frac{R^2}{4}\frac{\Delta P}{\mu L} = -\lambda\frac{R}{2}\frac{\Delta P}{\mu L} - \frac{R^2}{4}\frac{\Delta P}{\mu L} \tag{4.16}$$

Substituting A_1 and A_2 into the Eq. (4.12) yields,

$$u(r) = \frac{1}{4\mu}\frac{\Delta P}{L}(R^2 - r^2 + 4R^2Kn) \tag{4.17}$$

Calculating mean velocity,

$$u_m = \frac{\int_0^R \frac{1}{4\mu}\frac{\Delta P}{L}(R^2 - r^2 + 4R^2Kn)\,\pi r dr}{\int_0^R \pi r dr} = \frac{1}{8\mu}\frac{\Delta P}{L}R^2(1 + 8Kn) \tag{4.18}$$

Slip radius [43] is defined as below with choosing β_v=1.

$$\rho_s^2 = \frac{1}{1 + 4Kn} \tag{4.19}$$

Combining Eqs. (4.17), (4.18), and (4.19), the non dimensional velocity profile u^* becomes,

$$u^* = \frac{u}{u_m} = \frac{2\left(-\frac{r^2}{R^2} + 1 + 4Kn\right)}{1 + 8Kn} = \frac{\frac{2}{\rho_s^2}\left(1 - \frac{r^2}{R^2}\rho_s^2\right)}{\frac{2}{\rho_s^2} - 1} \tag{4.20}$$

$$= \frac{2}{2 - \rho_s^2}\left(1 - \frac{r^2}{R^2}\rho_s^2\right)$$

$$u^* = C_1\left(1 - \frac{r^2}{R^2}\rho_s^2\right) \tag{4.21}$$

where,

$$C_1 = \frac{2}{2 - \rho_s^2} \tag{4.22}$$

For a micro flow the velocity profile also depends on the Knudsen number. Note that, by setting Kn=0 velocity equation becomes identical to the fully developed velocity profile of a flow in a macrotube, which is

$$u^* = 2\left(1 - \frac{r^2}{R^2}\right) \tag{4.23}$$

4.2. Developing temperature distribution:

Energy Equation:

Again, for the flow conditions, steady state, and two dimensional flow, the governing Eqs. (3.5) and (3.6) can be written as Eqs (4.24) and (4.25) respectively.

$$\rho C_p\left(u\frac{\partial T}{\partial x} + v\frac{\partial T}{\partial r}\right) = k\left(\frac{\partial^2 T}{\partial x^2} + \frac{1}{r}\frac{\partial}{\partial r}\left(r\frac{\partial T}{\partial r}\right)\right) + \mu\Phi \tag{4.24}$$

$$\Phi = 2\left(\left(\frac{\partial u}{\partial x}\right)^2 + \left(\frac{1}{r}v\right)^2 + \left(\frac{\partial v}{\partial r}\right)^2\right) + \left(\frac{\partial v}{\partial x}\right)^2 + \left(\frac{\partial u}{\partial r} + \frac{\partial v}{\partial x}\right)^2 \tag{4.25}$$

As introduced before, for steady and fully developed flow u is a function of r only and the velocity component v is zero everywhere. As a result, Eq. (4.24) and Eq. (4.25) reduce to Eq. (4.26).

$$\rho C_p u \frac{\partial T}{\partial x} = \frac{k}{r}\frac{\partial}{\partial r}\left(r\frac{\partial T}{\partial r}\right) + k\frac{\partial^2 T}{\partial x^2} + \mu\left(\frac{\partial u}{\partial r}\right)^2 \tag{4.26}$$

On the right hand side of the Eq. (4.26), the second expression is axial conduction term and the third one is viscous dissipation term, which are not neglected in our study.

For constant wall temperature case, boundary conditions are,

$$r = 0, \qquad \frac{\partial T}{\partial r} = 0 \tag{4.27}$$

$$r = R, \qquad T - T_w = -\frac{2 - F_t}{F_t}\frac{2\gamma}{\gamma + 1}\frac{\lambda}{Pr}\left(\frac{\partial T}{\partial r}\right)_{r=R} \tag{4.28}$$

$$x = 0, \qquad T = T_i \tag{4.29}$$

Energy equation and the boundary conditions can be non-dimensionalized by the following dimensionless quantities.

$$\Theta = \frac{T - T_w}{T_i - T_w}, \qquad Br = \frac{\mu u_m^2}{k(T_i - T_w)}, \qquad \widetilde{Pe} = \frac{RePr}{\rho_s(2 - \rho_s^2)}$$
$$\xi = \rho_s^2(2 - \rho_s^2)\frac{x}{PeR}, \qquad \eta = \frac{r}{R}\rho_s, \qquad u^* = \frac{u}{u_m}, \tag{4.30}$$
$$\kappa = \frac{2 - F_t}{F_t}\frac{2\gamma}{\gamma + 1}\frac{1}{Pr}$$

In these equations, Θ is dimensionless temperature distribution, where T_i is initial temperature and T_w is wall temperature. Br, Brinkman number is a dimensionless group related to heat conduction from the wall to the flowing viscous fluid where μ is fluid dynamic viscosity, u_m is mean velocity and k is thermal conductivity. $\widetilde{Pe}$ is a dimensionless number relating the rate of advection of a flow to its rate of thermal diffusion where Re, Reynold number, is a measure of the ratio of inertial forces to viscous forces, Pr, Prandtl number, is a dimensionless number approximating the ratio of momentum diffusivity (kinematic viscosity) and thermal diffusivity, and ρ_s is slip radius. ξ is a dimensionless group for the axial coordinate where x is the axial coordinate in cylindrical coordinate system and R is the radius of tube. η is a dimensionless group for the radial coordinate where r is the radial coordinate in cylindrical coordinate system. κ is a constant where F_t is the thermal accommodation factor and γ is the specific heat ratio.

Introducing these dimensionless quantities into Eq. (2.26), the energy equation becomes,

$$\begin{aligned}\rho_s^2(2-\rho_s^2)\frac{u_m\rho C_p}{PeR}\frac{1}{2-\rho_s^2}(1-\eta^2)\frac{\partial\Theta}{\partial\xi} &= \rho_s^2\frac{k}{\eta R^2}\frac{\partial}{\partial\eta}\left(\eta\frac{\partial\Theta}{\partial\eta}\right)\\ +(\rho_s^2(2-\rho_s^2))^2\frac{k}{Pe^2R^2}\frac{\partial^2\Theta}{\partial\xi^2} &+ \rho_s^2\frac{\mu u_m^2}{R^2(T_i-T_w)}\left(\frac{\partial u^*}{\partial\eta}\right)^2\end{aligned} \tag{4.31}$$

$$\begin{aligned}\frac{1}{Pe}\frac{\rho u_m 2R}{\mu}\frac{\mu C_p}{k}(1-\eta^2)\frac{\partial\Theta}{\partial\xi} &= \frac{1}{\eta}\frac{\partial}{\partial\eta}\left(\eta\frac{\partial\Theta}{\partial r^*}\right)\\ +\rho_s^2(2-\rho_s^2)^2\frac{1}{Pe^2}\frac{\partial^2\Theta}{\partial\xi^2} &+ \frac{\mu u_m^2}{k(T_i-T_w)}\left(\frac{\partial u^*}{\partial\eta}\right)^2\end{aligned} \tag{4.32}$$

$$(1-\eta^2)\frac{\partial\Theta}{\partial\xi} = \frac{1}{\eta}\frac{\partial}{\partial\eta}\left(\eta\frac{\partial\Theta}{\partial\eta}\right) + \frac{1}{\widetilde{Pe}^2}\frac{\partial^2\Theta}{\partial\xi^2} + Br\left(\frac{\partial u^*}{\partial\eta}\right)^2 \tag{4.33}$$

By using the dimensionless quantities given in Eqs. (4.30), and the temperature jump boundary condition, Eqs. (4.27,28,29), the boundary conditions for constant wall temperature become,

$$\eta = 0, \qquad \frac{\partial \Theta}{\partial \eta} = 0 \tag{4.34}$$

$$\eta = \rho_s, \qquad \Theta = -\frac{2 - F_t}{F_t}\frac{2\gamma}{\gamma + 1}\frac{2Kn}{Pr}\rho_s \left(\frac{\partial \Theta}{\partial \eta}\right)_{\eta=\rho_s} = C_2 \rho_s \left(\frac{d\Theta}{d\eta}\right)_{\eta=\rho_s} \tag{4.35}$$

$$\xi = 0, \qquad \Theta = 1 \tag{4.36}$$

In this section, the effects of slip velocity and temperature jump are investigated separately. For this reason, parameter C_2 is defined for the temperature jump boundary condition as,

$$C_2 = -\frac{2 - F_t}{F_t}\frac{2\gamma}{\gamma + 1}\frac{2Kn}{Pr} = -2Kn\,\kappa \tag{4.37}$$

By using superposition, Θ can be decomposed as,

$$\Theta = \Theta_1 + \Theta_2 \tag{4.38}$$

$$\Theta_1 = f(\eta) \tag{4.39}$$

$$\Theta_2 = f(\eta, \xi) \tag{4.40}$$

Where $\Theta_1(\eta)$ is the fully developed temperature profile and $\Theta_2(\eta, \xi)$ is the solution of the homogeneous equation. Once Eq. (4.38) is substituted back to the energy equation, Eq. (4.33), the resulting equation for $\Theta_1(\eta)$ becomes, as $\xi \to \infty$, $\Theta \to \Theta_1(\eta)$,

$$\frac{1}{\eta}\frac{\partial}{\partial \eta}\left(\eta \frac{\partial \Theta_1}{\partial \eta}\right) = -\,Br\left(\frac{\partial u^*}{\partial \eta}\right)^2 \tag{4.41}$$

As the gradient of velocity is equal to,

$$\frac{\partial u^*}{\partial \eta} = -2C_1\eta \tag{4.42}$$

Equation (4.41) becomes,

$$\frac{1}{\eta}\frac{\partial}{\partial \eta}\left(\eta\frac{\partial \Theta_1}{\partial \eta}\right) = -4BrC_1^2\eta^2 \tag{4.43}$$

$\Theta_1(r^*)$ can be derived by integrating Eq. (4.43) together with the symmetry at the centerline and the temperature-jump at the wall boundary conditions as,

$$\frac{\partial}{\partial \eta}\left(\eta\frac{\partial \Theta_1}{\partial \eta}\right) = -4BrC_1^2\eta^3 \tag{4.44}$$

$$\frac{\partial \Theta_1}{\partial \eta} = -BrC_1^2\eta^3 + \frac{B_1}{\eta} \tag{4.45}$$

$$\Theta_1 = \frac{-BrC_1^2}{4}\eta^4 + B_1\ln(\eta) + B_2 \tag{4.46}$$

where the boundary conditions are,

$$\eta = 0, \qquad \frac{\partial \Theta_1}{\partial \eta} = 0 \tag{4.47}$$

$$\eta = \rho_s, \qquad \Theta_1 = C_2\rho_s\left(\frac{d\Theta_1}{d\eta}\right)_{\eta=\rho_s} \tag{4.48}$$

By applying the boundary conditions, B_1 and B_2 can be determined as below.

$$B_1 = 0 \tag{4.49}$$

$$B_2 = \frac{-BrC_1^2\rho_s^4}{4}(-1 + 4C_2) \tag{4.50}$$

As a result, $\Theta_1(\eta)$, the fully developed temperature profile is,

$$\Theta_1 = \frac{-BrC_1^2}{4}(\eta^4 - \rho_s^4 + 4\rho_s^4 C_2) \tag{4.51}$$

where C_1 and C_2 are defined through Eqs. (4.22) and (4.37), respectively.

For the homogeneous part of the temperature distribution, $\Theta_2(\eta)$, Eq. (4.52) should be solved together with the boundary conditions given below.

$$(1-\eta^2)\frac{\partial \Theta_2}{\partial \xi} = \frac{1}{\eta}\frac{\partial}{\partial \eta}\left(\eta \frac{\partial \Theta_2}{\partial \eta}\right) + \frac{1}{\widetilde{Pe}^2}\frac{\partial^2 \Theta_2}{\partial \xi^2} \tag{4.52}$$

$$\eta = 0, \qquad \frac{\partial \Theta_2}{\partial \eta} = 0 \tag{4.53}$$

$$\eta = \rho_s, \qquad \Theta_2 = C_2 \rho_s \left(\frac{d\Theta_2}{d\eta}\right)_{\eta=\rho_s} \tag{4.54}$$

$$\xi = 0, \qquad \Theta_2 = 1 - \Theta_1 \tag{4.55}$$

It is assumed that the solution to the above boundary value problem is of the form given by Eq. (4.56) [56]

$$\Theta_2 = Y(\eta)\exp(-\lambda^2 \xi) \tag{4.56}$$

where $Y(\eta)$ is a function of η only and λ is the eigenvalue.

Then, Eq. (4.52) becomes,

$$\frac{\partial^2 Y(\eta)}{\partial \eta^2} + \frac{1}{\eta}\frac{\partial Y(\eta)}{\partial \eta} + \lambda^2 \left((1-\eta^2) + \left(\frac{\lambda}{\widetilde{Pe}}\right)^2 \right) Y(\eta) = 0 \tag{4.57}$$

with the modified boundary conditions,

$$\eta = 0, \qquad \frac{\partial Y(\eta)}{\partial \eta} = 0 \tag{4.58}$$

$$\eta = \rho_s, \qquad Y(\eta) = C_2\, \rho_s \left(\frac{dY(\eta)}{d\eta}\right)_{\eta=\rho_s} \tag{4.59}$$

Note that, when $C_2 = 0$, and $\widetilde{Pe} = Pe$, the problem is equivalent to the macrochannel problem. Under symmetric boundary condition (4.58), the solution of equation (4.57) can be represented as,

$$Y(\eta) = g(\eta) \exp\left(-\lambda \frac{\eta^2}{2}\right) \tag{4.60}$$

By putting Eq. (4.60) into Eq. (4.57), Eq. (4.61) can be obtained.

$$\frac{\partial^2 g(\eta)}{\partial \eta^2} + \left(-2\lambda\eta + \frac{1}{\eta}\right)\frac{\partial g(\eta)}{\partial \eta} + \left(-2\lambda + \lambda^2 + \left(\frac{\lambda^2}{\widetilde{Pe}}\right)^2\right) \mathrm{g}(\eta) = 0 \tag{4.61}$$

Defining

$$z = x^2 = \lambda\eta^2 \tag{4.62}$$

Eq. (4.61) becomes,

$$\frac{\partial^2 g(x^2)}{\partial x^2} + \left(\frac{1}{\mathrm{x}} - 2\mathrm{x}\right)\frac{\partial g(x^2)}{\partial x} - 4\left(\frac{1}{2} - \frac{\lambda}{4} - \frac{\lambda^3}{4\widetilde{Pe}^2}\right) \mathrm{g}(x^2) = 0 \tag{4.63}$$

This is a Kummers confluent hypergeometric function in the form given in Ref. [57] as,

$$\frac{\partial^2 g(x^2)}{\partial x^2} + \left(\frac{2\mathrm{c}-1}{\mathrm{x}} - 2\mathrm{x}\right)\frac{\partial g(x^2)}{\partial x} - 4\mathrm{a}g(x^2) = 0 \tag{4.64}$$

With,

$$a = \frac{1}{2} - \frac{\lambda}{4} - \frac{\lambda^3}{4\widetilde{Pe}^2}$$
$$c = 1 \tag{4.65}$$

$$g(\eta) = 1F1(a, c; z) = \sum_{n=0}^{\infty} \frac{a_n}{c_n}\frac{z^n}{n!} \tag{4.66}$$

As a result, Eq. (4.60) becomes,

$$Y(\eta) = 1F1(a, c; \lambda\eta^2)\exp\left(-\lambda\frac{\eta^2}{2}\right) \tag{4.67}$$

By using second the boundary condition, Eq. (4.59), as,

$$\eta = \rho_s$$
$$1F1(a, c; \lambda\rho_s^2)(1 + C_2\lambda\rho_s^2) - \rho_s C_2 1F1'(a, c; \lambda\rho_s^2) = 0 \tag{4.68}$$

Eigenvalues of Eq. (4.67) can be found by the help of computer software Mathematica.

Note that eigenfunctions $Y(\eta)$ are not mutually orthogonal (by referring to the standard Sturm-Liouville problem) since the eigenvalues occur non-linearly. To determine coefficients A_n, one of the four different uses of Gram-Schmidt orthogonal

procedure can be applied. The main difference of all four orthogonalization processes is the computational time of finding the solution. However, method 4, given in the Appendix in detail, along with the other methods, is going to give different results then other three methods while the Pe number increases. This is the result of neglecting some terms in the calculation of α_{nj}.

After finding all eigenvalues, eigenfunctions and summation constants, temperature distribution Eq. (4.56) can be found as,

$$\Theta_2 = \sum_n A_n Y(\eta) \exp\left(-{\lambda_n}^2 \xi\right) \tag{4.69}$$

$$\Theta_2 = \sum_n A_n 1F1(a, c; \lambda_n \eta^2) \exp\left(-\lambda_n \frac{\eta^2}{2}\right) \exp\left(-{\lambda_n}^2 \xi\right) \tag{4.70}$$

Finally the temperature distribution is,

$$\Theta = \Theta_1 + \Theta_2 \tag{4.71}$$

$$\begin{aligned} \Theta = \frac{-Br C_1^2}{4}(\eta^4 - \rho_s^4 + 4\rho_s^4 C_2) \\ + \sum_n A_n 1F1(a, c; \lambda_n \eta^2) \exp\left(-\lambda_n \frac{\eta^2}{2}\right) \exp\left(-{\lambda_n}^2 \xi\right) \end{aligned} \tag{4.72}$$

Using an energy balance, the local heat transfer coefficient is written as,

$$q_s'' = -k\left(\frac{\partial T}{\partial r}\right)_{r=R} \tag{4.73}$$

$$q_s'' = h_x(T_m - T_w) \tag{4.74}$$

$$h_x = -\frac{k}{(T_m - T_w)}\left(\frac{\partial T}{\partial r}\right)_{r=R} \tag{4.75}$$

By introducing dimensionless quantities, Eq. (4.30), into Eq. (4.75), the Nusselt number is determined for constant wall temperature as,

$$Nu_\xi = \frac{h_\xi 2R}{k} = -\frac{2}{\Theta_m}\rho_s\left(\frac{\partial \Theta}{\partial \eta}\right)_{\eta=\rho_s} \tag{4.76}$$

where Θ_m is the dimensionless mean temperature, and it is defined as,

$$\Theta_m(\xi) = \frac{1}{\rho_s^2}\int_0^{\rho_s} u(\eta)\,\Theta(\eta,\xi)\eta d\eta \tag{4.77}$$

In some of the results part, classical dimensionless quantities Eq. (4.78) are used to make comparison with literature.

$$x^* = \frac{x}{R\,Pe}, \qquad r^* = \frac{r}{R} \tag{4.78}$$

The solution procedure is prepared by the help of Mathematica software. Eigenvalues are found by built in function root finder combined with a bracketing method. The method works up to a very high number of eigenvalues with high accuracy and short CPU times. However, for the orthogonalization part, the procedure is going to be complicated because of the oscillating characteristic of high order eigenfunctions. Integration of eigenfunctions results in excessive CPU time which is not practical. This problem is eliminated by using Gaussian quadrature method for integrations. Gaussian integration with 100 points and 12 weights gives nearly the same result with direct integration in a relatively short time.

CHAPTER 5

RESULTS

The problem is solved for different cases to obtain a variety of results for different conditions. First, both hydrodynamically and thermally fully developed flow, then hydrodynamically developed, thermally developing flow are solved for macro and micro cases separately. Axial conduction and viscous dissipation effects are also investigated individually in different sub-sections. The outcomes are shown using tables and graphs. Comparisons with similar solutions are indicated clearly. Some useful results are also tabulated and given in the Appendix.

5.1. Results for both hydrodynamically and thermally fully developed flow:

Fully developed flow in a macropipe and a micropipe are investigated separately to see the validity of the solution by comparing it with well-known solutions from literature and to find the effect of axial conduction and viscous dissipation on fully developed Nusselt number, Nu_{fd}. Nusselt number values are presented as a function of Peclet, Brinkman, and Knudsen numbers. Since the number of eigenfunctions used in the summation solution does not affect the fully developed Nu, only the first eigenvalues are used to find Nu_{fd}.

5.1.1. Solution for macro flow (Kn=0):

In this section, boundary conditions for macro flow; no slip velocity and no temperature jump, are used to solve the problem for the continuum case. The main

objective is to show the validity of solution procedure through a comparison with literature.

Axial conduction effect

Axial conduction effect appears in the Kummers hypergeometric function part of the infinite series solution of the eigenvalue problem. It directly influences eigenvalues and eigenfunctions by the change in Pe values. As mentioned before, just the first eigenvalues and eigenfunctions are enough to calculate Nu_{fd}. To investigate the effect of axial conduction on fully developed macro flow, Nu_{fd} for different Pe values are shown in table 4 using the first eigenvalues for each Pe value. It is seen from table 4 that for $Pe=10^9$, which corresponds to a high magnitude of the thermal energy convected to the fluid relative to the thermal energy conducted axially within the fluid, Nu is equal to 3.66 with three significant figures, which is exactly the same with all other analytical solutions that excluded axial conduction in literature for laminar fully developed flow in a pipe. The results are so accurate that even the smallest effect of axial conduction depicts itself in the Nu values. Furthermore, it is important that the effect of each different Pe value is included in the calculation of eigenvalues and eigenfunctions. In brief, one can conclude that Nu_{fd} decreases from 4.18 at Pe=0 to 3.66 at $Pe=\infty$. Also, solution shows the axial conduction effect up to Pe equal to 10^6. However the effect is so insignificant that axial conduction can be neglected for Pe values higher than 100.

Table 4 Fully developed Nu for different Pe values with Kn=0, Br=0 and κ=1.667

Pe	Nu_{fd}	λ_1	Pe	Nu_{fd}	λ_1	Pe	Nu_{fd}	λ_1
10^9	3.65679	2.70436	70	3.65771	2.70185	0.8	4.05359	1.29972
10^6	3.65679	2.70436	60	3.65803	2.70094	0.7	4.06747	1.22567
1000	3.6568	2.70435	50	3.65858	2.69945	0.6	4.08189	1.144
900	3.6568	2.70435	40	3.65957	2.69671	0.5	4.09685	1.05284
800	3.6568	2.70435	30	3.66168	2.69085	0.4	4.11239	0.94938
700	3.6568	2.70434	20	3.66754	2.6746	0.3	4.12852	0.828904
600	3.65681	2.70433	10	3.69518	2.59693	0.2	4.14526	0.682326
500	3.65681	2.70431	8	3.71247	2.54742	0.1	4.16263	0.486419
400	3.65682	2.70429	6	3.74302	2.45812	0.04	4.17337	0.309143
300	3.65684	2.70423	5	3.76729	2.3853	0.03	4.17518	0.267943
200	3.65691	2.70406	4	3.80153	2.27947	0.02	4.177	0.218953
100	3.65724	2.70313	2	3.92236	1.86754	0.01	4.17882	0.154949
90	3.65735	2.70284	1	4.02735	1.42981	0.001	4.18047	0.049035
80	3.65749	2.70244	0.9	4.04022	1.36744	10^{-6}	4.18065	0.001551

Table 5 Comparison of fully developed Nu for different Pe with those from literature with Kn=0, Br=0 and κ=1.667

	Pe = 1.0			Pe = 2.0			Pe = 5.0			Pe = 10		
	Nu_{fd}	Nu_{fd}^{*}	Nu_{fd}^{**}	Nu_{fd}	Nu_{fd}^{*}	Nu_{fd}^{**}	Nu_{fd}	Nu_{fd}^{*}	Nu_{fd}^{***}	Nu_{fd}	Nu_{fd}^{*}	Nu_{fd}^{**}
	4.027	4.028	4.030	3.922	3.922	3.925	3.767	3.767	3.767	3.695	3.695	3.697
Error	0%	0.2%	0.7%	0%	0%	0.8%	0%	0%	0%	0%	0%	0.5%

Nu_{fd} : Results for the present study

Nu_{fd}^{*} : Results from Cetin et al [58]

Nu_{fd}^{**} : Results from Shah and London [10]

Nu_{fd}^{***}: Results from Lahjomri and Qubarra [59]

Table 5 presents a comparison of current results for Nu with those available from literature. As seen therein, the results are reliable for the fully developed case and the error is less than 1%. All the results can be compared with table 2.

Axial conduction and viscous dissipation effects

For fully developed macro flow, since viscous dissipation term dominates heat transfer, Nu_{fd} converges to the well-known Nu of 9.60 regardless of the values of Pe and Br numbers. As a result, axial conduction term has no influence on Nu_{fd} for the cases with viscous dissipation included. Also, the effect of negative Br or positive Br or even the value of Br cannot be visualized for the fully developed case; as mentioned before, Br signifies the importance of the viscous heating relative to the conductive heat transfer.

5.1.2. Solution for micro flow with slip flow boundary conditions:

Slip flow regime is defined as the range of Kn between 0.001 and 0.1. Temperature jump (Eq. (1.4)) and slip velocity (Eq. (1.3)) boundary conditions are added into the solution to eliminate non-continuum effects of micro flow.

Axial conduction effect

Similar to the previous case, only the first eigenvalues are used since the number of eigenfunctions added to the summation does not affect the Nu_{fd}.

Axial conduction effect for fully developed micro flow is presented in table 6 for slip flow case for κ=1.667. It can be seen that axial conduction still has a high influence on Nu_{fd} for different Kn values. However, its effect decreases as Kn increases. It can also be concluded that the effect of Kn is higher for low Pe values because of high axial conduction resulting in an increase of dimensionless temperature at any cross section such as in the boundaries. In slip flow regime, temperature gradients at the

boundaries are the main influential part for temperature jump boundary condition. As a result, for low Pe values, temperature gradients and the resulting temperature jump at the pipe wall make Kn have a high effect on flow.

Again table 6 shows the effect of axial conduction for high Pe in slip flow. Axial conduction effect for different Kn is negligible for Pe higher than 100.

Table 6 Fully developed Nu values and first eigenvalues for different Pe and Kn with Br=0 and κ=1.667

κ=1.667	**Pe=1**		**Pe=2**		**Pe=5**		**Pe=10**	
	Nu_{fd}	**λ_1**	**Nu_{fd}**	**λ_1**	**Nu_{fd}**	**λ_1**	**Nu_{fd}**	**λ_1**
Kn=0	4.02735	1.42981	3.92236	1.86754	3.76729	2.3853	3.69518	2.59693
Kn=0.001	4.02081	1.4276	3.91568	1.86484	3.76029	2.38236	3.68795	2.59409
Kn=0.02	3.84645	1.38931	3.74634	1.81726	3.59679	2.32816	3.52614	2.53989
Kn=0.04	3.60307	1.35573	3.51677	1.7741	3.38693	2.27492	3.32512	2.48331
Kn=0.06	3.34365	1.3279	3.27265	1.73711	3.16562	2.22589	3.11463	2.4286
Kn=0.08	3.09265	1.30487	3.03537	1.70544	2.94922	2.18118	2.90842	2.37681
Kn=0.10	2.8608	1.28579	2.8148	1.67833	2.74607	2.1407	2.71385	2.3285
κ=1.667	**Pe=50**		**Pe=60**		**Pe=100**		**Pe=1000**	
	Nu_{fd}	**λ_1**	**Nu_{fd}**	**λ_1**	**Nu_{fd}**	**λ_1**	**Nu_{fd}**	**λ_1**
Kn=0	3.65858	2.69945	3.65803	2.70094	3.65724	2.70313	3.6568	2.70435
Kn=0.001	3.65121	2.69673	3.65067	2.69823	3.64987	2.70042	3.64942	2.70165
Kn=0.02	3.48987	2.64353	3.48933	2.64505	3.48854	2.64727	3.48809	2.64851
Kn=0.04	3.29322	2.58562	3.29274	2.58712	3.29205	2.58932	3.29166	2.59054
Kn=0.06	3.08834	2.52788	3.08795	2.52933	3.08737	2.53146	3.08705	2.53265
Kn=0.08	2.88748	2.47199	2.88717	2.47338	2.88672	2.47542	2.88646	2.47655
Kn=0.10	2.69747	2.41904	2.69723	2.42036	2.69687	2.42229	2.69667	2.42337

With the light of table 6, one can conclude that Nu_{fd} decreases with an increase in Kn because of temperature jump at the pipe walls. Temperature jump at $\eta = 1$ (pipe wall) for Pe=1 and ξ=1 can be seen in Fig. 2 for air, which presents the temperature profiles for different Kn values at ξ=1 with Pe=1, Br=0 and κ=1.667.

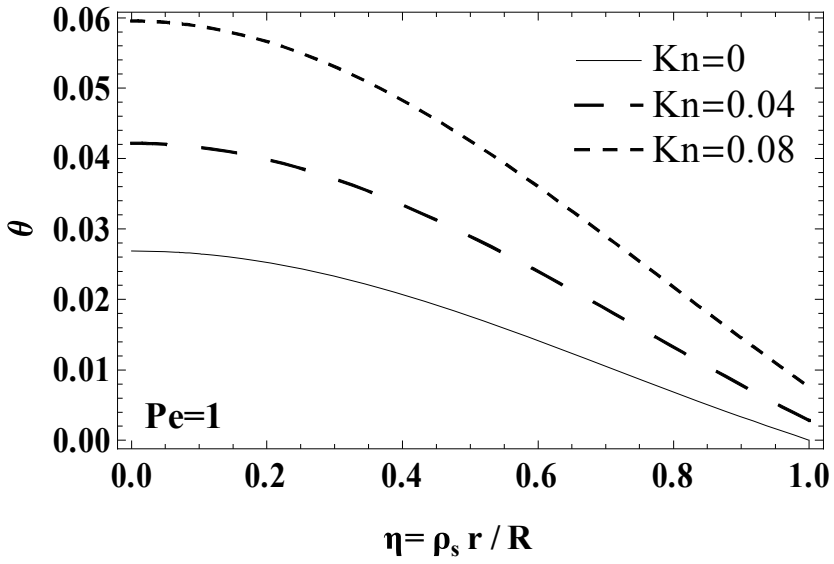

Figure 2 Temperature profiles for different Kn values at $\eta=\rho_s$ with Pe=1, Br=0 and κ=1.667

In this section, the effects of slip velocity and temperature jump are investigated separately. In slip-flow regime two main parameters; Kn and the parameter κ, affect the temperature profile. Kn includes the effect of rarefaction and the parameter κ includes the effect of gas and surface properties. $\kappa = 0$ and $\kappa = 10$ are two limiting cases for this section as stated by Larrode et al [43]. $\kappa = 0$ is a fictitious, but a useful case to observe the effect of slip velocity without temperature jump on heat transfer. $\kappa = 10$ is the other limit, which accounts for a very large temperature jump at the wall. $\kappa = 1.667$ is the typical value for air, which is the working fluid for various engineering application and is taken so in this study, except this section.

Table 7 shows the effect of temperature jump more clearly for the slip flow regime. Including velocity slip and no temperature jump ($\kappa=0$) boundary conditions results in higher Nu with increasing Kn. However, as mentioned before, including the temperature jump decreases Nu for Kn higher than 0. By increasing the parameter κ, temperature jump also increases, such that for the limiting case ($\kappa=10$), Nu decreases to 0.84 from 3.66.

Table 7 Fully developed Nu with Br=0 for different Kn and κ values.

Pe=1000	**Nu_{fd}**		
	κ =0	**κ =1.667**	**κ =10**
Kn=0	3.6568	3.6568	3.6568
Kn=0.001	3.66769	3.64942	3.56013
Kn=0.02	3.85559	3.48809	2.2911
Kn=0.04	4.02067	3.29166	1.62371
Kn=0.06	4.15989	3.08705	1.2465
Kn=0.08	4.27886	2.88646	1.00768
Kn=0.10	4.38166	2.69667	0.843998

As a result, the solution shows perfectly the effect of Kn on Nu_{fd} for different Pe and temperature jump amounts. Results are sensible for small changes in effect of axial conduction as tabulated for different Pe values. Table 8 summarizes and compares the slip flow regime results for different Pe, Kn, and κ values. Comparison with literature shows the validity of outcomes.

Table 8 Comparison of fully developed Nu with Br=0 with literature for different Kn and κ.

κ	Pe=1		Pe=2		Pe=5		Pe=10		Pe=1000		
	Nu_{fd}	Nu_{fd}^*	Nu_{fd}	Nu_{fd}^*	Nu_{fd}	Nu_{fd}^*	Nu_{fd}	Nu_{fd}^*	Nu_{fd}	Nu_{fd}^*	Kn
0	4.02735	4.028	3.92236	3.922	3.76729	3.767	3.69518	3.695	3.6568	3.656	**0.00**
1.667	4.02735	4.028	3.92236	3.922	3.76729	3.767	3.69518	3.695	3.6568	3.656	
10	4.02735	4.028	3.92236	3.922	3.76729	3.767	3.69518	3.695	3.6568	3.656	
0	4.35828	4.358	4.27026	4.270	4.13156	4.131	4.06096	4.061	4.02067	4.020	**0.04**
1.667	3.60307	3.604	3.51677	3.517	3.38693	3.387	3.32512	3.325	3.29166	3.292	
10	1.70548	1.706	1.6781	1.678	1.64315	1.643	1.62987	1.630	1.62371	1.624	
0	4.58445	4.585	4.50912	4.509	4.38553	4.386	4.31884	4.319	4.27886	4.279	**0.08**
1.667	3.09265	3.093	3.03537	3.036	2.94922	2.949	2.90842	2.909	2.88646	2.887	
10	1.02919	1.029	1.02097	1.021	1.01186	1.012	1.00892	1.009	1.00768	1.008	

Nu_{fd} : Results for the present study

Nu_{fd}^* : Results from Cetin et al [58]

Axial conduction and viscous dissipation effects

Similar to macro flow, for the fully developed case, viscous dissipation term dominates heat transfer, such that Nu_{fd} converges to the same value for all Pe and Br values in the slip flow regime. Again, axial conduction term has no influence on Nu_{fd} when viscous dissipation is included. However, for micro flow, Nu_{fd} decreases with an increase in Kn, which is mainly the result of slip velocity at boundaries in the slip flow regime. As a result of slip velocity different than 0 at the pipe boundaries, velocity gradients near the pipe wall reduce. As mentioned before, velocity gradients especially near the pipe wall are the main effective factor for viscous dissipation, such that a decrease of velocity gradients results in the decrease of viscous heating. Table 9 shows the variation of Nu_{fd} with different Kn for =1000 and κ=1.667.

Table 9 Fully developed Nu values for different Br and Kn with Pe=1000 and κ=1.667

	κ=1.667	**Br**						
	Pe=1000	**-0.1**	**-0.05**	**-0.01**	**0**	**0.01**	**0.05**	**0.1**
Nu_{fd}	**Kn=0**	9.6	9.6	9.6	3.6568	9.6	9.6	9.6
	Kn=0.001	9.46357	9.46357	9.46357	3.64942	9.46357	9.46357	9.46357
	Kn=0.02	7.42759	7.42759	7.42759	3.48809	7.42759	7.42759	7.42759
	Kn=0.04	6.0315	6.0315	6.0315	3.29166	6.0315	6.0315	6.0315
	Kn=0.06	5.06509	5.06509	5.06509	3.08705	5.06509	5.06509	5.06509
	Kn=0.08	4.35926	4.35926	4.35926	2.88646	4.35926	4.35926	4.35926
	Kn=0.10	3.82252	3.82252	3.82252	2.69667	3.82252	3.82252	3.82252

Table 9 furthermore shows that the effect of negative Br or positive Br or even the value of Br cannot be observed for the fully developed case in slip flow regime similar to the continuum case. Again, as can be seen in table 10, the comparison

shows perfect agreement with available results from literature for all Br different than 0.

Table 10 Comparison of fully developed Nu with Br≠0 for different Kn with literature.

	Br≠0	
Kn	**Nu_{fd}**	**Nu_{fd}^***
0.00	9.6	9.6
0.04	6.03	6.03
0.08	4.36	4.36

Nu_{fd} : Approximate results for the present study

Nu_{fd}^* : Results from Cetin et al [60]

5.2. Results for hydrodynamically developed, thermally developing flow:

Accuracy of the method for the thermally developing region mainly depends on the number of eigenvalues and eigenfunctions used in the summation solution. Especially as the solution gets closer to the entrance region, more and more eigenfunctions are needed for an accurate calculation. However, a high number of eigenfunctions for a summation solution is still a problem and not practical for today's computers. Therefore, the first objective is to determine the exact number of eigenfunctions for a suitable range of ξ through which the results can be examined. However, in this section, non-dimensional term x^* is used to make comparison with literature. For this purpose, local Nu as a function of x^* and number of eigenfunctions used in summation solution, N, is plotted in Fig. 3 for Pe=1 with Kn=0, Br=0 and κ=1.667.

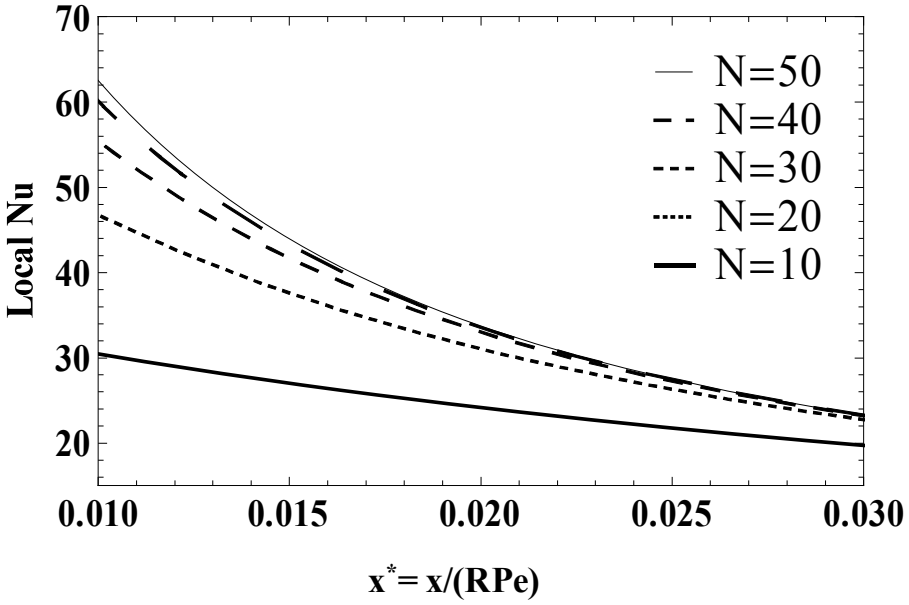

Figure 3 Deviation of local Nu with N, the number of eigenfunctions used in the solution, for Pe=1 with Kn=0, Br=0 and κ=1.667

After a thorough investigation, it is seen that solutions with 50, 40 and 30 eigenfunctions give the same results after x^*= 0.02. Since practical microchannels have high length to diameter ratio, the resolution at the inlet does not play an important role for the overall picture. As a result 30 eigenfunctions are enough to see the deviation of local Nu along dimensionless axial direction x^* greater than 0.02.

5.2.1. Solution for macro flow (Kn=0):

Similar to the case in section 4.1.1 for macro flow, no slip velocity and no temperature jump boundary conditions are used to solve the problem for the continuum case. By excluding the effects of axial conduction and viscous dissipation, the problem transforms into the basic thermal development problem, which is the classical Graetz problem.

Table 11 shows the comparison of the present results for the classical Graetz problem excluding axial conduction, viscous dissipation, and rarefaction effects. Results are exactly same with those from Ref. [61] for $x^*>0.01$, which is an acceptable range for the present study. Therefore, selecting the number of eigenfunctions as 30 is a suitable choice. If fewer eigenfunctions are used, the discrepancy from literature is going to increase, since the early entrance region needs more eigenfunctions for more accurate results. The temperature profile approach is improper to model this part of the entrance region. A simpler profile such as the Leveque Solution can solve this portion easily as mentioned in chapter 2.

Table 11 Comparison of local Nu for the present study with those from Ref. [61] for Pe=1000, Kn=0, Br=0 and κ=1.667

x^*	Nu_x	Nu_x^*	x^*	Nu_x	Nu_x^*	x^*	Nu_x	Nu_x^*
0.0001	23.5207	22.275	0.002	8.0685	8.0362	0.03	3.89466	3.8942
0.0002	18.4569	17.558	0.003	7.06137	7.0432	0.04	3.76912	3.7689
0.0003	15.8100	15.277	0.004	6.44161	6.4296	0.05	3.7101	3.7100
0.0004	14.1864	13.842	0.005	6.01025	6.0015	0.06	3.6821	3.6820
0.0005	13.0678	12.824	0.006	5.68788	5.6812	0.07	3.66881	3.6688
0.0006	12.2343	12.050	0.007	5.4355	5.4301	0.08	3.66249	3.6624
0.0007	11.5795	11.433	0.008	5.23133	5.2269	0.09	3.6595	3.6595
0.0008	11.0459	10.926	0.009	5.0621	5.0584	0.1	3.65808	3.6580
0.0009	10.5990	10.498	0.01	4.9192	4.9161	0.15	3.65683	3.6568
0.001	10.2171	10.130	0.02	4.17344	4.1724	0.2	3.65680	3.6568

Nu_{fd} : Results for present study

Nu_{fd}^* : Results from Shah [61]

It can also be seen from table 11 that the flow reaches the fully developed condition after $x^* = 0.15$, which is also exactly the same with the thermal entrance length of a classical laminar pipe flow.

Axial conduction effect

For the investigation of the axial conduction effect in the thermally developing region for macro flow, 30 eigenvalues and their eigenfunctions are found for each Pe value, since each one has different eigenvalues and eigenfunctions as a result of axial conduction effect. Table 20 in the appendix shows the first 30 eigenvalues for different Pe values. For all cases, more detailed tables are presented in the appendix.

Temperature profiles, through ξ^* for different Pe, can be seen in Fig. 4. Increase of the thermal entrance length, L_t, with a decrease in Pe can be visualized clearly. Decrease of Pe increases the axial conduction, which results in the rise of dimensionless temperature at any cross section and length required to achieve fully developed conditions.

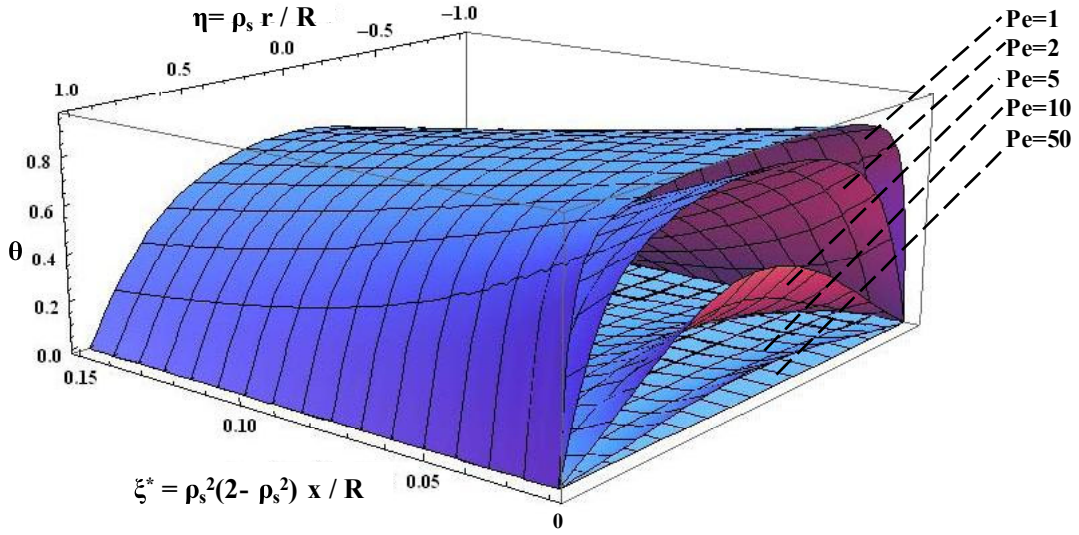

Figure 4 Temperature profiles for different Pe with Kn=0, Br=0 and κ=1.667

Furthermore, L_t values for different Pe are tabulated in table 12. Since the Nu results are displayed with 5 significant figures in this study, during the calculation of L_t, Nu_{fd} results with 6 significant figures are used to reach fully developed condition.

Table 12 Thermal entrance length, L_t, for different Pe with Kn=0, Br=0 and κ=1.667

Kn=0, Br=0	**Pe=1**	**Pe=2**	**Pe=5**	**Pe=10**	**Pe=50**
L_t ($\xi^* = \rho_s^2(2-\rho_s^2)\, x / R$)	2.272	0.585	0.098	0.03	0.004

Figure 5-a and b show the local Nu along the dimensionless axis x^* and ξ^* for different Pe, respectively. By the help of dimensionless x^*, comparison with Hennecke [27] (table 3) shows the validation of the solution such that the small differences with data points taken from [27] can be visualized in Fig. 5-a. Moreover, local Nu through ξ^* for different Pe are tabulated in table 13. Similar to fully developed results, Nu increases with decreasing Pe. Furthermore, axial conduction effect is more influential at the beginning of the development part and its effect decreases with an increase in Pe. Again, streamwise conduction effect reduces while Nu converges to the fully developed value. As a result, it can be concluded that axial conduction is more important for the early part of thermal development region.

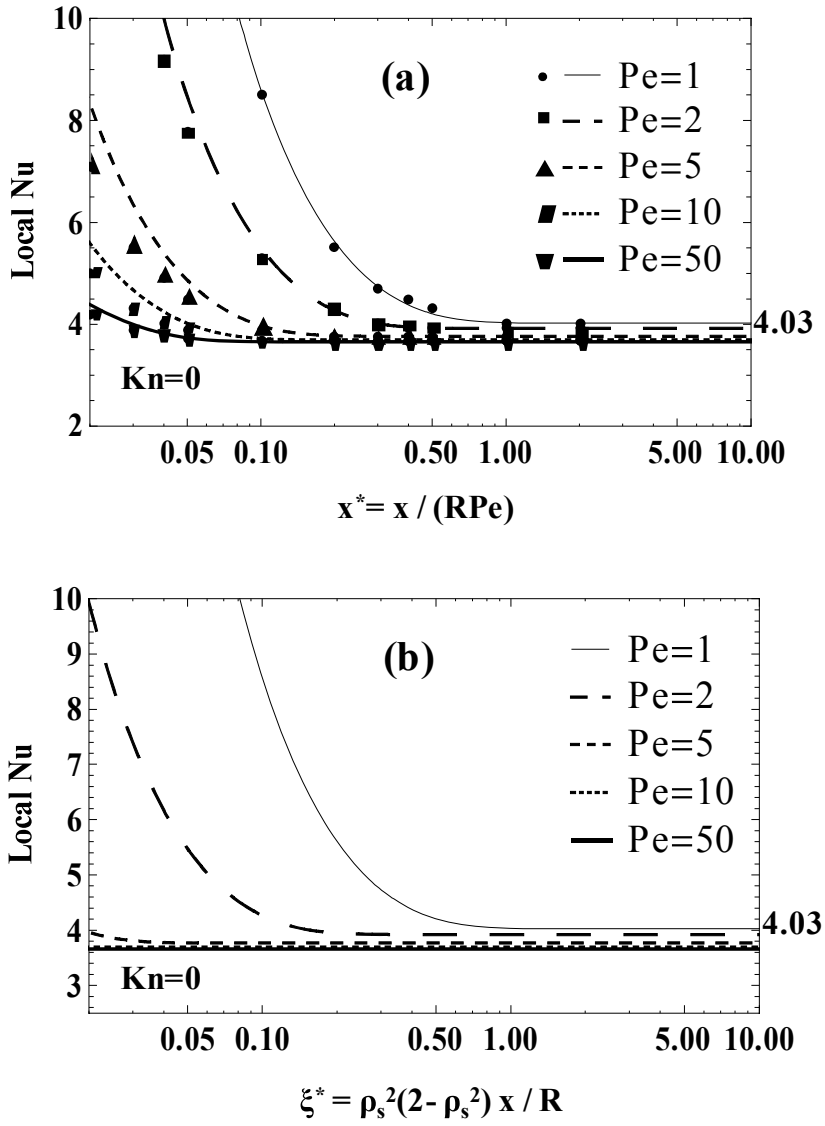

Figure 5 Variation of Local Nu along (a) x^* (with data points from Hennecke) and (b) ξ^* for different Pe with Kn=0, Br=0 and $\kappa = 1.667$

Table 13 Local Nu along the entrance region for different Pe with Kn=0, Br=0 and κ=1.667

$\xi^* = \rho_s^2(2-\rho_s^2)\, x / R$	$Nu_{x,T}$				
	Pe=1	**Pe=2**	**Pe=5**	**Pe=10**	**Pe=50**
0.01	55.6042	17.7366	4.81184	3.72045	3.65858
0.02	33.0403	9.93414	3.96441	3.69538	3.65858
0.03	23.1657	7.39902	3.81108	3.69518	3.65858
0.04	17.9617	6.17572	3.77732	3.69518	3.65858
0.05	14.814	5.47368	3.7696	3.69518	3.65858
0.06	12.7188	5.03003	3.76782	3.69518	3.65858
0.07	11.2282	4.73232	3.76741	3.69518	3.65858
0.08	10.1158	4.52438	3.76732	3.69518	3.65858
0.09	9.25542	4.37504	3.7673	3.69518	3.65858
0.1	8.57144	4.26563	3.76729	3.69518	3.65858
0.2	5.60473	3.94821	3.76729	3.69518	3.65858
0.3	4.73626	3.92446	3.76729	3.69518	3.65858
0.4	4.37611	3.92253	3.76729	3.69518	3.65858
0.5	4.20596	3.92238	3.76729	3.69518	3.65858
0.6	4.12062	3.92236	3.76729	3.69518	3.65858
0.7	4.07655	3.92236	3.76729	3.69518	3.65858
0.8	4.05343	3.92236	3.76729	3.69518	3.65858
0.9	4.04122	3.92236	3.76729	3.69518	3.65858
1.0	4.03473	3.92236	3.76729	3.69518	3.65858
2.0	4.02736	3.92236	3.76729	3.69518	3.65858
3.0	4.02735	3.92236	3.76729	3.69518	3.65858
4.0	4.02735	3.92236	3.76729	3.69518	3.65858

Axial conduction and viscous dissipation effects

Influence of both axial conduction and viscous dissipation is investigated in this section. Viscous heating has no effect on eigenvalues and eigenfunctions, thus the values obtained in the last section are used (table 20 in the appendix).

L_t values for different Br presented in table 14. Nu_{fd} is chosen as 9.6 for all Br values different than 0 during the calculation of L_t. Increase in Br for positive values and decrease for negative values result in shortening of the length of obtaining Nu as 9.6.

Table 14 Thermal entrance length, L_t, for different Br with Pe=1, Kn=0 and κ=1.667

Pe=1, Kn=0	**Br=0.01**	**Br=0.001**	**Br=0**	**Br= - 0.001**	**Br= - 0.01**
L_t ($\xi^* = \rho_s^2(2-\rho_s^2)\, x / R$)	4.783	5.348	2.272	5.348	4.787

Figure 6 and table 15 show the effect of different Br values on Nu for Pe=1 case. First of all, Nu values are the same with no viscous dissipation case up to some portion of ξ^* depending on Br value. The main effect of viscous heating starts after that point and dominates the flow. Nu converges the same value, 9.6, for all Br values different than 0. This can be visualized in figure 6 more clearly.

As mentioned before, for positive Br, which means fluid cooling, viscous dissipation enhances the heat transfer. This can be seen from the sudden increase of Nu (jump point) around ξ^* =1 and ξ^* =3 in Fig. 6 and table 15. Furthermore, the increase of Br results in movement of the jump-point in the downstream direction like the increase of L_t which is the main effect of value of Br. For negative Br, which means fluid heating, Nu goes to infinity at singular points where the bulk mean temperature of the fluid is equal to wall temperature. Again the value of Br alters the location of singular points as a result of change of viscous dissipation. After the singular points, heat transfer changes direction as mentioned before. Singular points of negative Br case can be visualized from Fig. 6 and table 15 more clearly.

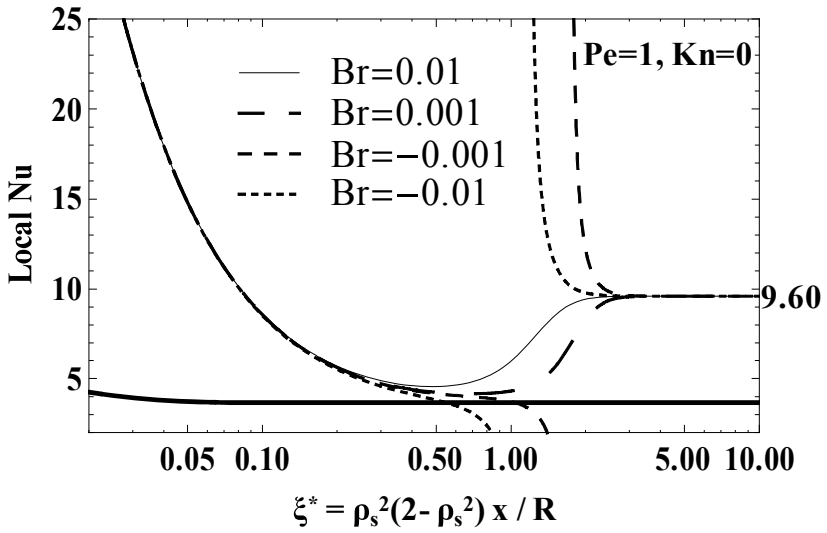

Figure 6 Variation of Local Nu along ξ^* for different Br with Pe=1, Kn=0 and $\kappa = 1.667$

Table 15 Local Nu along the entrance region for different Br with Pe=1, Kn=0 and κ=1.667

$\xi^* = \rho_s^2(2-\rho_s^2)\, x / R$	$Nu_{x,T}$				
	Br=0.01	**Br=0.001**	**Br=0**	**Br= - 0.001**	**Br= - 0.01**
0.01	55.5977	55.6036	55.6042	55.6049	55.6107
0.02	33.0384	33.0401	33.0403	33.0404	33.0421
0.03	23.1698	23.1661	23.1657	23.1653	23.1616
0.04	17.9714	17.9627	17.9617	17.9607	17.9519
0.05	14.829	14.8155	14.814	14.8125	14.7989
0.06	12.7387	12.7208	12.7188	12.7168	12.6988
0.07	11.2529	11.2307	11.2282	11.2257	11.2034
0.08	10.1451	10.1187	10.1158	10.1128	10.0863
0.09	9.28925	9.25881	9.25542	9.25202	9.22132
0.1	8.60975	8.57529	8.57144	8.56759	8.53278
0.2	5.69019	5.61336	5.60473	5.59608	5.51732
0.3	4.88214	4.75113	4.73626	4.72133	4.58398
0.4	4.606	4.39986	4.37611	4.35219	4.12868
0.5	4.55476	4.2427	4.20596	4.16877	3.81278
0.6	4.63693	4.1766	4.12062	4.06358	3.4966
0.7	4.82439	4.16106	4.07655	3.98952	3.07176
0.8	5.1115	4.1802	4.05343	3.92083	2.38073
0.9	5.49708	4.23028	4.04122	3.83872	1.06409
1.0	5.97231	4.31483	4.03473	3.72385	-2.1161
2.0	9.43046	8.26116	4.02736	12.1837	9.78376
3.0	9.59707	9.57062	4.02735	9.62974	9.60298
4.0	9.59995	9.59951	4.02735	9.6005	9.60005
5.0	9.6	9.59999	4.02735	9.60001	9.6
6.0	9.6	9.6	4.02735	9.6	9.6

Axial conduction in the presence of viscous heating still has a high effect through the thermally developing region up to some value of ξ^* depending on Pe value. For Pe=1 axial conduction determines the local Nu up to ξ^* =0.5 after which viscous dissipation starts to influence the flow and dominates the Nu_{fd} as mentioned before. Before that point, Nu values are similar to no viscous dissipation case. Furthermore, the main impact of Pe is on the jump point location (sudden increase of Nu) in the thermally developing region, which can be seen in figure 7. Increase in Pe results in movement of jump point towards downstream, similar to the influence of Br values. However, its effect is more influential than effect of Br values. Table 16 presents the local Nu values for different Pe with Br=0.01.

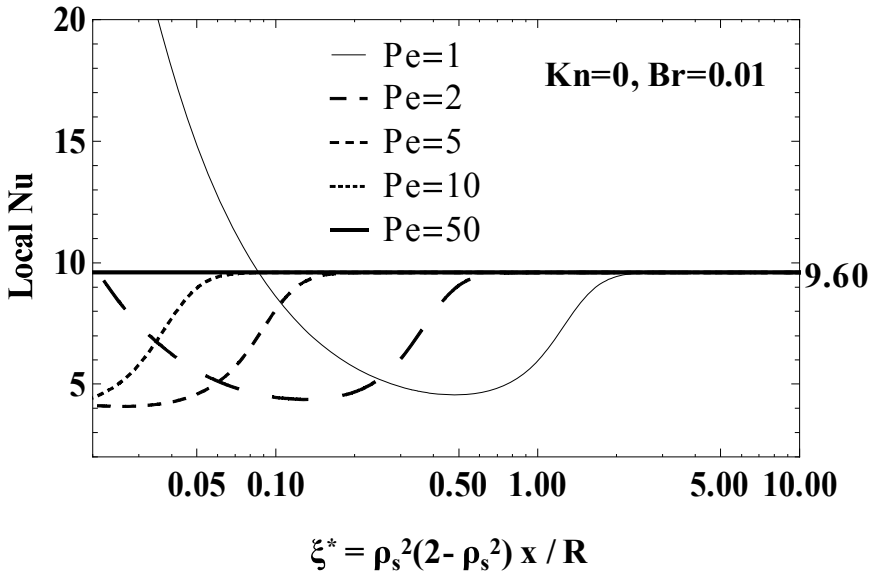

Figure 7 Variation of Local Nu along ξ^* for different Pe with Br=0.01, Kn=0 and κ=1.667

Table 16 Local Nu along the entrance region for different Pe with Br=0.01, Kn=0 and κ=1.667

$\xi^* =$ $\rho_s^2(2-\rho_s^2)\, x / R$	$Nu_{x,T}$				
	Pe=1	**Pe=2**	**Pe=5**	**Pe=10**	**Pe=50**
0.01	55.5977	17.7491	4.89316	3.93464	9.2313
0.02	33.0384	9.96509	4.12586	4.44646	9.59973
0.03	23.1698	7.4462	4.09772	5.81853	9.6
0.04	17.9714	6.23886	4.26816	7.73341	9.6
0.05	14.829	5.55339	4.58521	8.96748	9.6
0.06	12.7387	5.12753	5.06947	9.42169	9.6
0.07	11.2529	4.84926	5.73099	9.55266	9.6
0.08	10.1451	4.66284	6.5245	9.58764	9.6
0.09	9.28925	4.5375	7.34242	9.59679	9.6
0.1	8.60975	4.45497	8.06401	9.59917	9.6
0.2	5.69019	4.67765	9.59296	9.6	9.6
0.3	4.88214	6.04871	9.59998	9.6	9.6
0.4	4.606	7.93694	9.6	9.6	9.6
0.5	4.55476	9.07139	9.6	9.6	9.6
0.6	4.63693	9.45914	9.6	9.6	9.6
0.7	4.82439	9.56443	9.6	9.6	9.6
0.8	5.1115	9.59114	9.6	9.6	9.6
0.9	5.49708	9.5978	9.6	9.6	9.6
1.0	5.97231	9.59946	9.6	9.6	9.6
2.0	9.43046	9.6	9.6	9.6	9.6
3.0	9.59707	9.6	9.6	9.6	9.6
4.0	9.59995	9.6	9.6	9.6	9.6
5.0	9.6	9.6	9.6	9.6	9.6
6.0	9.6	9.6	9.6	9.6	9.6

5.2.2. Solution for micro flow with slip flow boundary conditions:

Again, for slip flow regime defined as the range of Kn between 0.001 and 0.1, temperature jump and slip velocity boundary conditions are added into the solution to eliminate the non-continuum effects of micro flow.

Axial conduction effect

Similar to the previous sections, 30 eigenvalues and their eigenfunctions are found for each Pe to investigate the axial conduction effect through the thermally developing region of the slip flow regime. Table 21 and 22 in the appendix shows the first 30 eigenvalues for different Pe values.

Temperature profiles, along ξ^* for different Kn values, can be seen in Fig. 8. As mentioned before, the main influence of Kn on temperature profile for slip flow regime is the temperature jump at the pipe wall that can be seen in Fig. 8 more clearly. Temperature jump at the boundaries increases with increase in Kn.

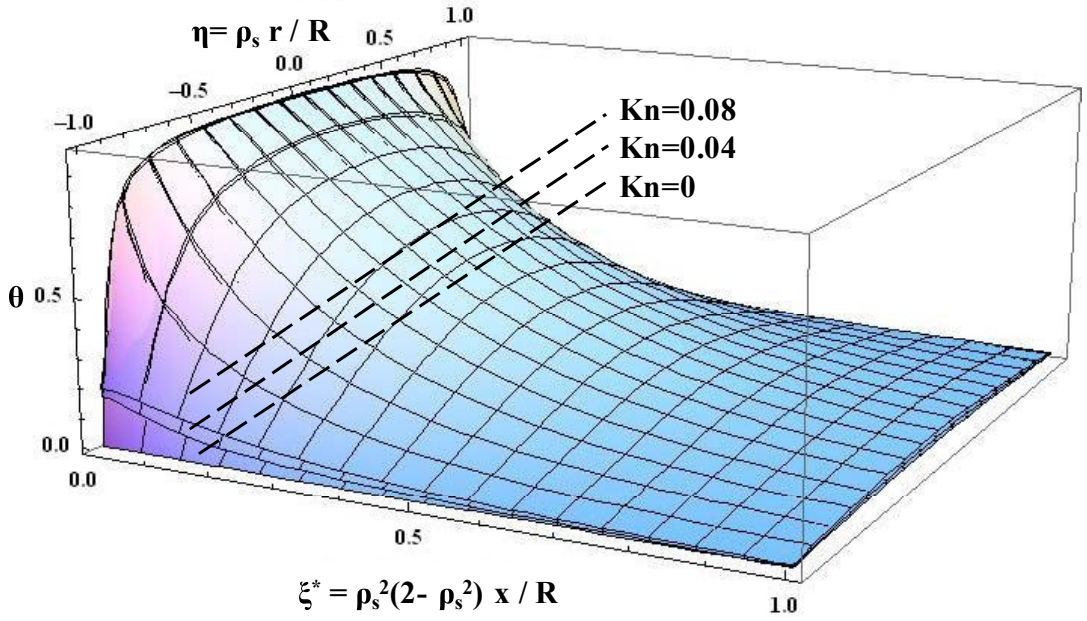

Figure 8 Temperature profiles for different Kn with Pe=1, Br=0 and κ=1.667

L_t values for different Kn are presented in table 17, but they can also be visualized more clearly in tables 23 and 24 in the appendix where local Nu values are tabulated for thermally developing region of slip flow. Kn value has little influence on L_t and its effect further decreases with increase in Pe.

Table 17 Thermal entrance length, L_t, for different Pe and Kn with Br=0 and κ=1.667

	Br=0	**Pe=1**	**Pe=2**	**Pe=5**	**Pe=10**	**Pe=50**
L_t ($\xi^* = \rho_s^2(2-\rho_s^2)\, x / R$)	**Kn=0**	2.272	0.585	0.098	0.03	0.004
	Kn=0.04	2.426	0.622	0.105	0.03	0.004
	Kn=0.08	2.383	0.601	0.105	0.03	0.004

Figure 9 and 10 show the variation of Nu for several Pe values for Kn=0.04 and Kn=0.08, respectively. The effect of axial conduction for the slip flow case still has a high influence on Nu for different Kn values. However, its effect decreases as Kn increases. Also we can conclude that effect of Kn is emphasized for low Pe values.

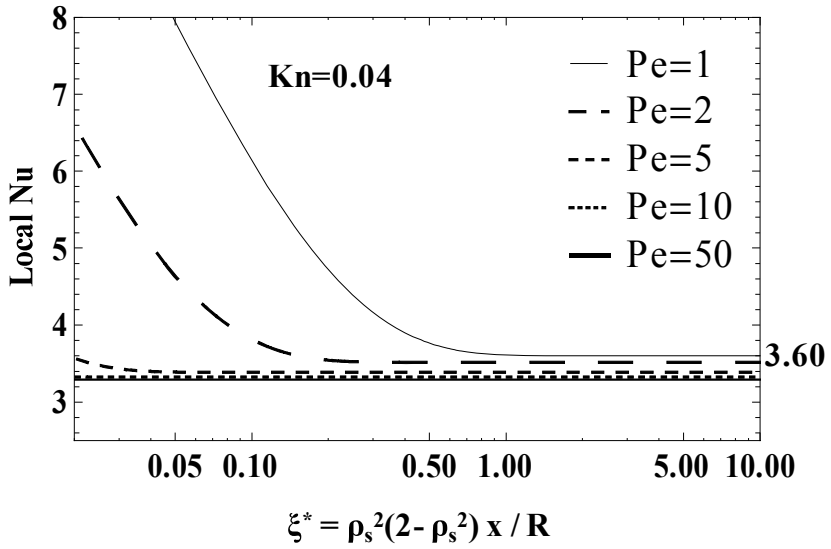

Figure 9 Variation of local Nu along ξ^* for different Pe with Kn=0.04, Br=0 and κ = 1.667

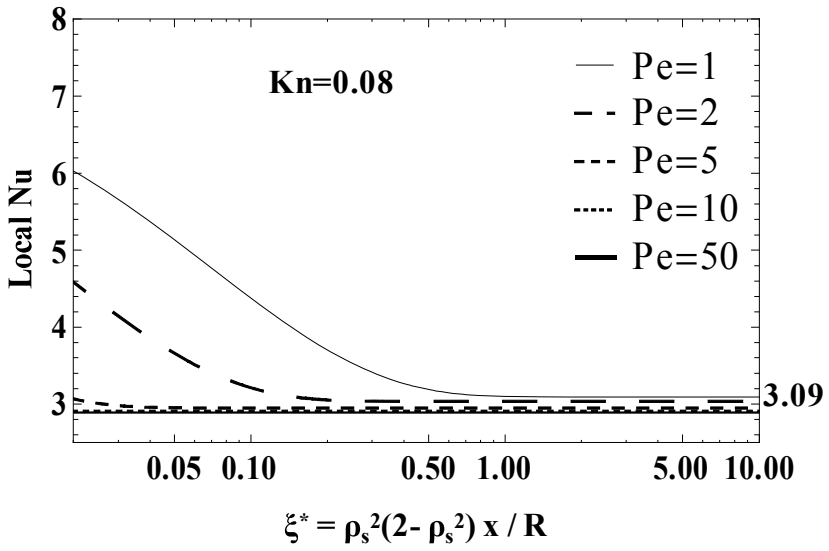

Figure 10 Variation of local Nu along ξ^* for different Pe with Kn=0.08, Br=0 and $\kappa = 1.667$

As a conclusion for this section, it can be said that Nu decreases with an increase in Kn because of temperature jump at the pipe walls in the slip flow regime. Result can also be visualized in tables 23 and 24 in the appendix.

Axial conduction and viscous dissipation effects

For the influence of both axial conduction and viscous dissipation in the thermally developing region of slip flow regime, the same eigenvalues and eigenfunctions evaluated in last section are used (tables 21 and 22, see appendix), since viscous heating has no effect on eigenvalues and eigenfunctions.

Table 19 shows L_t values for Br=0.01. Contradictory to the last section, Kn effect on L_t cannot be neglected. Increase in Kn results in increase of L_t.

Table 18 Thermal entrance length, L_t, for different Kn with Pe=1, Br=0.01 and κ=1.667

Pe=1, Br=0.01	Kn=0	Kn=0.04	Kn=0.08
L_t ($\xi^* = \rho_s^2(2-\rho_s^2)\, x / R$)	4.783	5.046	5.285

Furthermore, similar to the no viscous heating section, Nu decreases with an increase in Kn. Again similar to the macro case including viscous dissipation, Nu values converge to a value independent of Pe or Br values. However, different from macro flow, the dominant effect of viscous heating is reduced as a result of velocity slip boundary condition in micro flow, and fully developed Nu values decrease with an increase in Kn as mentioned before. Also, the increase in Kn results in the transition of jump point towards upstream, similar to L_t. Figure 11 and table 20 present the local Nu values for different Kn. Moreover, axial conduction effect for slip flow regime is the same as continuum case in the presence of viscous dissipation.

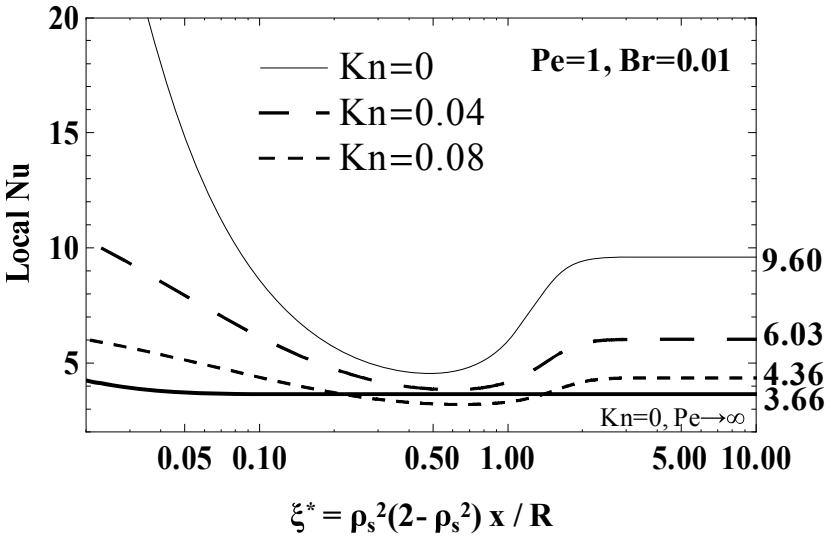

Figure 11 Variation of local Nu along ξ^* for different Kn with Pe=1, Br=0.01 and κ = 1.667

Table 19 Local Nu along the entrance region for different Kn with Pe=1, Br=0.01 and κ=1.667

$\xi^* = \rho_s^2(2-\rho_s^2)\, x / R$	$Nu_{x,T}$		
	Kn=0	**Kn=0.04**	**Kn=0.08**
0.01	55.5977	11.814	6.53171
0.02	33.0384	10.341	6.0312
0.03	23.1698	9.31616	5.66383
0.04	17.9714	8.5467	5.37534
0.05	14.829	7.94123	5.13954
0.06	12.7387	7.44962	4.9417
0.07	11.2529	7.04138	4.77261
0.08	10.1451	6.69655	4.62607
0.09	9.28925	6.40135	4.4977
0.1	8.60975	6.14589	4.38426
0.2	5.69019	4.74507	3.71503
0.3	4.88214	4.20965	3.43057
0.4	4.606	3.97271	3.295
0.5	4.55476	3.87283	3.23139
0.6	4.63693	3.84883	3.20759
0.7	4.82439	3.87513	3.20887
0.8	5.1115	3.94155	3.22861
0.9	5.49708	4.04485	3.26426
1.0	5.97231	4.18405	3.31526
2.0	9.43046	5.84792	4.18502
3.0	9.59707	6.02648	4.35259
4.0	9.59995	6.03138	4.35904
5.0	9.6	6.0315	4.35926
6.0	9.6	6.0315	4.35926

CHAPTER 6

SUMMARY, CONCLUSIONS AND FUTURE WORK

Steady state heat transfer problem for hydrodynamically developed, thermally developing micro tube flow is studied by including axial conduction and viscous dissipation. Analytical solution is obtained to increase the fundamental understanding of the physics of the problem. Kummers hypergeometric functions are used in the solution of the problem, and it was seen that the use of these functions are very effective by the help of Mathematica software. Very good agreement is obtained with the available results in the literature.

Closed-form solutions are important for the investigation of the effect of each parameter by a physical aspect, but they have some disadvantages over numerical solutions. First of all, it is hard to obtain an analytical solution for a complex problem of a complex geometry where numerical methods can be very useful. Secondly, analytical solutions are suitable only for the condition of problem for which the solution was prepared, but numerical ones can be used for conditions different than the initial one. Even though numerical methods are applicable for wide range of conditions, it should be noted that they are estimations for exact solutions, which can be obtained only by analytical ones.

A wide variety of results are found for different conditions. Eigenvalues, used in summation solutions, temperature distributions, fully developed and local Nu values and the thermal entrance lengths are shown by tables or graphs for all these cases as function of Pe, Kn, κ and Br.

The effects of four parameters; Pe, Kn, κ and Br, on the flow are discussed. Pe, varying between 1 and ∞, represent the dependency of the flow upon downstream locations. Kn ranges from Kn =0, which is the continuum case (i.e. flow in macro tubes), to Kn =0.1, which is the upper limit of the slip flow regime. κ parameter ranges from κ =0, which is a fictious case introducing the effect of rarefaction only on the velocity, to κ =10, which is also a fictious case standing for a large temperature jump at the wall. For most of the parts κ =1.667 is discussed frequently, since it is the typical value for air, the working fluid for most of the engineering applications. Br is ranging from 0, which stands for the case without viscous dissipation, to Br =0.01.

Results show that axial conduction has an important effect for low Pe and increases with a decrease in Pe value. However, it is negligible for Pe higher than 100. Increase in axial conduction, increases both Nu_{fd} and local Nu values for all continuum (macro) and slip flow (micro), fully developed or thermally developing cases without viscous dissipation. Moreover, L_t also increases as a result of increase in axial conduction. However, different from macro flow, the high effect of axial conduction for Pe<100 decreases as a result of enhancement of rarefaction effect in micro flow because of high streamwise conduction.

In the presence of viscous dissipation, axial conduction has no effect on Nu_{fd} but still effects the local Nu values up to some ξ^* depending on the Pe value. Before that point viscous dissipation starts to influence the flow, local Nu values are similar with no viscous dissipation case. Again, similar to its effect on L_t, the increase of axial conduction results in movement of jump point (sudden increase of Nu) towards upstream for the Br values different than 0 in both macro and micro cases.

For viscous dissipation, results show that Nu_{fd} converges to 9.6 regardless of Pe or Br values for all conditions in continuum case. Only through the thermally developing region, effect of Br values can be visualized. For positive Br, viscous heating enhances the heat transfer. However, negative values result in singular

points, after which heat transfer changes direction. Moreover, the value of Br has an effect on the jump point, the increase of Br value results in movement of jump point towards downstream similar to its effect on L_t, independent of its sign. All of the outcomes are also valid for the slip flow regime. However, different from macro flow, the dominant effect of viscous heating is reduced as a result of velocity slip boundary condition in micro flow and fully developed Nu values decrease with an increase in Kn. Moreover, L_t also increases as a result of an increase in Kn, which also means movement of jump point towards upstream.

For all cases, the rarefaction effect decreases the Nu values in slip flow regime in the case of parameter κ and Kn different than 0. Rarefaction is investigated by parameter κ and Kn. Parameter κ only has an effect on temperature jump boundary condition such that the increase of κ results in a decrease in Nu for a fixed Kn value different than 0. For κ=0, no temperature jump case, main effect of temperature jump can be understood more clearly. For this case Nu values increase with an increase in Kn as a result of slip velocity in the slip flow regime. However, practically, κ values would be different than 0 that κ =1.667 is discussed frequently, since it is the typical value for air, for most of the parts in this study.

It should be remarked again that the solution is in a closed form and can reveal any change in variables. However, the closed form equation is not presented because of its impractical length. From this study, the following general conclusions can be obtained.

(1) Axial conduction should not be neglected for Pe values less than 100 for all continuum (macro) and slip flow (micro), fully developed or thermally developing cases without viscous dissipation.

(2) In the presence of viscous dissipation, axial conduction should not be neglected for short pipes with Pe values less than 100.

(3) For viscous heating case; even for small Br, fully developed Nu value experiences a jump in magnitude. The value of the Br only affects the axial location of the jump. Therefore, the effect of viscous heating should be considered even for small Br with a large length over diameter (L/D) ratios, which is the case for flows in micropipes.

(4) For a fixed κ parameter, the deviation from continuum increases with increasing rarefaction.

(5) For a fixed Kn, the deviation from continuum increases with increasing κ parameter.

(6) For all κ values different than 0, both local and fully developed Nu values decrease with an increase in Kn.

This study considers axial conduction, viscous dissipation and rarefaction effects in microtubes for constant wall temperature boundary condition. For future works, constant heat flux boundary condition can be applied to the problem. Also, the same problem can be solved for microchannels with different cross-sections. Furthermore, to understand the flow better, some further effects in addition to axial conduction, viscous dissipation, and rarefaction such as; axial conduction at the pipe wall, variation of thermophysical properties, compressibility effect, different geometrical configurations, different thermal boundary conditions, can be included in the analysis.

REFERENCES

1. Kakac, S., Yener, Y., *Convective Heat Transfer*. 1980, Ankara: METU.

2. Beskok, A., Karniadakis, G.E., *Simulation of Heat and Momentum Transfer in Complex Micro-Geometries.* Journal of Thermophysics Heat Transfer 1994. **8**: p. 355-370.

3. Gad-el-Hak, M., *The MEMS Handbook*. 2001, New York: CRC Press.

4. Eckert, E.G.R., Drake, R.M. Jr., *Analysis of Heat and Mass Transfer*. 1972, New York: McGraw-Hill.

5. Graetz, L., *Uber die Warmeleitungsfahigkeit von Flussigkeiten (On the thermal conductivity of liquits). Part 1.* Ann. Phys. Chem., 1883. **18**: p. 79-94.

6. Nusselt, W., *Die Abhangigkeit der Warmeubergangszhal von der Rohrlange (The Dependence of the Heat Transfer Coefficient on the Tube Length).*. VDI Z. , 1910. **54**: p. 1154-1158.

7. Kakac, S., Shah, R. K., *Handbook of Single Phase Convective Heat Transfer*. 1987, A Wiley-Interscience: New York.

8. Larkin, B.K., *High-Order Eigenfuntions of the Graetz Problem.* The American Institute of Chemical Engineers, 1961. **7**: p. 530.

9. Brown, G.M., *Heat or Mass Transfer in a Fluid in Laminar Flow in a Circular or Flat Conduit.* The American Institute of Chemical Engineers, 1960. **6**: p. **179-183**.

10. Shah, R.K., London, A.L. , *Laminar Flow Forced Convection in Ducts*. 1978, New York: Academic Press.

11. Leveque M. A., *Les lois de la transmission de chaleur par convection.* Ann. Mines, 1928. **13**: p. 201-299, 305-362, 381-415.

12. Acrivos, A., *The extended Graetz problem at low Peclet numbers.* Applied Scientific Research, 1980. **36**: p. 35-40.

13. Vick, B., Ozisik, M. N.,Bayazitoglu, Y., *A Method of Low Peclet Number Thermal Entry Region Problems with Axial Conduction.* Letters in Heat and Mass Transfer, 1980. **7**: p. 235-248.

14. Vick, B., Ozisik, M. N.,Bayazitoglu, Y., *An Exact Analysis of Low Peclet Number Heat Transfer in Laminar Flow with Axial Conduction.* Letters in Heat and Mass Transfer, 1981. **8**: p. 1-10.

15. Hsu, C.J., *An Exact Analysis of Low Peclet Number Thermal Entry Region Heat Transfer in Transversely Non-Uniform Velocity Field.* The American Institute of Chemical Engineers, 1971. **17**: p. 732-740.

16. Papoutsakis, E., Ramkrishna, D.,Lim, H. C., *The Extended Graetz Problem with Dirichlet Wall Boundary Condition.* Applied Scientific Research, 1980. **36**: p. 13-34.

17. Papoutsakis, E., Ramkrishna, D.,Lim, H. C., *The Extended Graetz Problem with Prescribed Wall Flux.* The American Institute of Chemical Engineers, 1980. **26**: p. 779-787.

18. Verhoff, F.H., Fisher, D. P., *A Numerical Solution of the Graetz Problem with Axial Conduction.* Journal Heat Transfer, 1973. **95**: p. 12-134.

19. Lahjomri, J., Qubarra, A., *Analytical Solution of the Gratez Problem with Axial Conduction.* J Heat Transfer, 1999. **121**: p. 1078-1083.

20. Michelsen, M.L., Villadsen, J., *The Graetz Problem with Axial Heat Conduction.* Int. J. Heat Mass Transfer, 1974. **17**: p. 1391-1402.

21. Ash, R.L., Heinbockel, J. H., *Note on Heat Transfer in Laminar Fully Developed Pipe Flow with Axial Conduction.* Math. Phys., 1970. **21**: p. 266-269.

22. Taitel, V., Tamir, A., *Application of the Integral Method to Flows with Axial Conduction.* Int. J. Heat Mass Transfer, 1972. **15**: p. 733-740.

23. Taitel, V., Bentwich, M., Tamir, A., *Effects of Upstream and Ddownstream Boundary Conditions on Heat(Mass) Transfer with Axial Diffussion.* Int. J. Heat Mass Transfer, 1973. **16**: p. 359-369.

24. Ash, R.L., Heinbockel, J. H., *Personal communication of London and Shah.*, in *Old Dominion University, Norfolk, Virginia*.

25. Ash, R.L., Heinbockel, J. H., *Note on Heat Transfer in Laminar, Fully Developed Pipe Flow with Axial Conduction.* Z. Angew. Math. Phys. , 1970. **21**(166-169).

26. Pahor, S., Strand, J., *Die Nusseltsche Zahl fur laminare Stromung im zylindrischen Rohr mit konstanter Wandtemperature.* Z. Angew. Math. Phys., 1956. **7**: p. 536-538.

27. Hennecke, D.K., *Heat Transfer by the Hagen-Poiseuille Flow in the Thermal Development Regime with Axial Conduction.* Waerme- Stoffuebertrag, 1968. **1**: p. 177-184.

28. Kader, B.A., *Heat and mass transfer in laminar flow in the entrance region section of a circular tube.* High Temp. (USSR), 1971. **9**: p. 1115-1120.

29. Labuntsov, D.A., *Heat Emission in Pipes During Laminar Flow of a Liquid with Axial Heat Conduction Taken into Account.* Sov. Phys. Dokl., 1958. **3**: p. 33-35.

30. Singh, S.N., *Heat Transfer by Laminar Flow in a Cylindrical Tube.* Appl. Sci. Res., 1958. **A7**: p. 325-340.

31. Millsaps, K., Pohlhausen, K. *Heat Transfer for Hagen Poiseuille Flows*. in *Differential Equations*. 1956. Collage Park.

32. Schmidt, F.W., Zeldin, B., *Laminar Heat Transfer in the Entrance Region of Ducts.* Applied Scientific Research, 1970. **23**: p. 73-94.

33. Brinkman, H.C., *Heat Effects in Capillary Flow.* Appl. Sci. Res., 1951. **A2**(120-124).

34. Ou, J.W., Cheng, K. C., *Viscous Dissipation Effect Thermal Entrance Heat Transfer in Laminar and Turbulent Pipe Flows with Uniform Wall Tempearture.* Am. Ins. Aeronaut. Astron. Pap., 1974: p. 74-743.

35. Ou, J.W., Cheng, K. C., *Effect of Pressure Work and Viscous Dissipation on Graetz Problem for Gas Flows in Parallel Plate Channels.* Waerme-Stoffuebertrag, 1973. **6**: p. 191-198.

36. Sobhan, C.B., Garimella, S.V., *A Comparative Analysis of Studies on Heat Transfer and Fluid Flow in Microchannels.* Microscale Thermophysical Engineering 2001. **5**(293-311).

37. Choi, S.B., Barron, R. F., Warrington, R. O. ,, *Fluid Flow And Heat Transfer In Microtubes, Micromechanical Sensors, Actuators, And Systems.* ASME DSC, 1991. **32**: p. 49-60.

38. Phafler, J., Harley, J., Bau, H. H., Zemel, J. , , *Gas and Liquid Flow In Small Channels, Micromechanical Sensors, Actuators, And Systems.* ASME DSC 1991. **32**: p. 49-60.

39. Kavehpour, H.P., Faghri, M., Asako, Y., *Effects of Compressibility and Rarefaction on Gasseous Flows in Microchannels.* Numerical Heat Transfer, 1997. **A 32**: p. 677-696.

40. Arkilic, E.B., Breuer, K. S., Schmidt, M. A., *Gaseous Flow in Microchannels. Application of Microfabrication to Fluid Mechanics.* ASME FED, 1994. **197**: p. 57-66.

41. Barron, R.F., Wang, X., Warrington, R. O., Ameel, T. , *Evaluation of the Eigenvalues for the Graetz Problem in Slip Flow.* Int. Comm. Heat Mass Transfer 1996. **23 (4)**: p. 1817-1823.

42. Barron, R.F., Wang, X., Ameel, T. A., Warrington, R. O.,, *The Graetz Problem Extended To Slip-flow.* Int. J. Heat Mass Transfer, 1997. **40(8)**: p. 1817-1823.

43. Larrode, F.E., Housiadas, C., Drossinos, Y., *Slip Flow Heat Transfer in Circular Tubes.* Int. J. Heat Mass Transfer, 2000. **43**: p. 2669-2680.

44. Mikhailov, M.D., Vulchanov, N. L., *A Computational Procedure for Strum-Liouville Problems.* J. Comp. Phys, 1983: p. 827-835.

45. Mikhailov, M.D., Cotta, R. M., *Integral Transform Method for Eigenvalue Problems.* Num. Meth. Eng., 1997. **10**: p. 827-835.

46. Mikhailov, M.D., Cotta, R. M., Kakac, S., *Steady State and Periodic Heat Transfer in Micro Conduits*, in *Micro-Scale Heat Transfer: Fundamentals and Applications in Biological and Microelectromechanical systems*. 2005, Springer Netherlands. p. 49-74. Editors: Kakaç et al.

47. Cetin, B., Yuncu, H.,Kakac, S., *Gaseous Flow in Microchannels with Viscous Dissipation.* Int J Transport Phenomena, 2006. **8**: p. 297-315.

48. Xu, B., Ooi, K. T.,Mavriplis, C.,Zaghloul, M. E., *Evaluation of Viscous Dissipation in Liquid Flow in Microchannels.* J. Micromech. Microeng., 2003. **13**: p. 53-57.

49. Morini, G.L., *Viscous Heating in Liquid Flows in Microchannels.* Int. J. Heat Mass Transfer, 2005. **48**: p. 391-392.

50. Tunc, G., Bayazitoglu, Y., *Heat Transfer in Microtubes with Viscous Dissipation.* Int. J. Heat Mass Transfer, 2001. **44**: p. 2395-2403.

51. Tunc, G., Bayazitoglu, Y. *Convection at the Entrance of Micropipes with Sudden Wall Temperature Change*. in *Institution of Mechanical Engineers*. 2002. New Orleans, Lousiana.

52. Hadjiconstantinou, N.G., Simek, O., *Constant Wall Temperature Nusselt Number in Micro and Nano-channels.* J. Heat Transfer, 2002. **124**: p. 356-364.

53. Jeong, H.E., Jeong, J. T., *Extended Graetz Problem Including Streamwise Conduction and Viscous Dissipation in Microchannel* International Journal of Heat and Mass Transfer, 2006. **49**(13-14): p. 2151-2157.

54. Cotta, R.M., Kakac, S., Mikhailov, M. D., Castelloes, F. V.,Cardoso, C. R., *Transient Flow and Thermal Analysis in Microfluidics* in *Microscale Heat Transfer Fundamentals and Applications*. 2005, Springer Netherlands. p. 175-196. Editors: Kakaç et al.

55. Horiuchi, K., Dutta, P., Hossain, A., *Joule-Heating Effects in Mixed Electroosmotic and Pressure-Driven Microflows under Constant Wall Heat Flux.* J. Engineering Mathematics, 2006. **54**(159-180).

56. Dutta, P., Horiuchi, K., Yin, H. M., *Thermal Characteristics of Mixed Electroosmotic and Pressure-Driven Microflows.* Computers & Mathematics with Applications 2006. **52**(5): p. 651-670.

57. Arkfen, G.B., Weber, H. J., *Mathematical Methods For Physicists*. 2005: Academic Press. 796-799.

58. Cetin, B., Yazicioglu, A. G., Kakac, S., *Fluid Flow in Microtubes with Axial Conduction Including Rarefaction and Viscous Dissipation.* International Communication in Heat and Mass Transfer, 2008. **35**: p. 535-544

59. Lahjomri, J., Qubarra, A., *Analytical Solution of the Graetz Problem with Axial Conduction.* J Heat Transfer, 1999. **121**: p. 1078-1083.

60. Cetin, B., *Analysis of Single Phase Convective Heat Transfer in Microtubes and Microchannels*, in *Mechanical Engineering*. 2005, Middle East Technical University: Ankara. p. 28-33.

61. Shah, R.K., *Thermal Entry Length Solutions for the Circular Tube and Parallel Plates*, in *Proc. Natl. Heat Mass Transfer Conf.* 1975: Bombay.

APPENDIX

GRAM SCHMIDT ORTHOGONAL PROCEDURE

In this part of the study, non-orthogonal eigenfunctions, Y_n, are turned into orthogonalized functions, f_n. Four different methods are utilized for this purpose which are described by some relations as

$$Y_n = our\ function\ (non-orthogonal)$$

$$f_n = orthogonalized\ function$$

$$\emptyset_n = orthonormalized\ function$$

$$\int_0^1 f_i f_j\, d\eta = \{\begin{matrix} \int_0^1 f_i^2 d\eta & if\ i = j \\ 0 & if\ i \neq j \end{matrix}\} \tag{6.1}$$

$$\int_0^1 \emptyset_i \emptyset_j\, d\eta = \{\begin{matrix} 1 & if\ i = j \\ 0 & if\ i \neq j \end{matrix}\} \tag{6.2}$$

$$\emptyset_i = \frac{f_i}{\sqrt{\int_0^1 f_i^2 d\eta}} \tag{6.3}$$

Method 1

Let us assume a series of orthogonal functions f_n and orthonormal function $\emptyset_n$ related to our functions as,

$$f_1 = Y_1 \tag{6.4}$$

$$f_2 = Y_2 - \alpha_{21}\emptyset_1 \tag{6.5}$$

$$f_3 = Y_3 - \alpha_{31}\emptyset_1 - \alpha_{32}\emptyset_2 \tag{6.6}$$

$$\vdots$$

$$f_n = Y_n - \sum_{j=1;n\geq 2}^{n-1} \alpha_{nj}\emptyset_j \tag{6.7}$$

where α_{nj} are constants. The next step is to obtain these constants in order to find the orthogonal function f_n. From the property of orthogonal functions (Eq. (6.1)) and orthonormal functions (Eq. (6.2)), we can write the following relationship as

$$f_2 = Y_2 - \alpha_{21}\emptyset_1 \tag{6.8}$$

$$\int_0^1 f_2\emptyset_1 d\eta = \int_0^1 Y_2\emptyset_1 d\eta - \alpha_{21}\int_0^1 \emptyset_1\emptyset_1 d\eta \tag{6.9}$$

$$0 = \int_0^1 Y_2\emptyset_1 d\eta - \alpha_{21}1 \tag{6.10}$$

$$\alpha_{2,1} = \int Y_2\emptyset_1 d\eta \tag{6.11}$$

As a result

$$\alpha_{n,j} = \int Y_n \emptyset_j d\eta \tag{6.12}$$

Then, the calculation of summation constants B_n for orthogonal functions f_n,

$$\Theta = \Theta_1 + \Theta_2 \tag{6.13}$$

$$\Theta_2 = \Theta - \Theta_1 = \sum A_n Y_n \exp(-\lambda^2 \zeta) = \sum B_n f_n \exp(-\lambda^2 \zeta) \tag{6.14}$$

The boundary condition at x=0 is

$$x = 0, \qquad \Theta = 1 \tag{6.15}$$

$$\left(1 - \frac{-BrC_1^2 \rho_s^4}{4}(r^4 - 1 + 4C_2)\right) = \sum A_n Y_n = \sum B_n f_n \tag{6.16}$$

$$B_n = \frac{\int_0^1 \left(1 - \frac{-BrC_1^2 \rho_s^4}{4}(r^4 - 1 + 4C_2)\right) f_n d\eta}{\int_0^1 f_n^2 d\,\eta} \tag{6.17}$$

Then summation coefficients A_n can be found by the help of software Mathematica with the relation as

$$\sum A_n Y_n = \sum B_n f_n \tag{6.18}$$

Method 2:

Let us assume a series of orthogonal functions f_n related to our functions as,

$$f_1 = Y_1 \tag{6.19}$$

$$f_2 = Y_2 - \alpha_{21} f_1 \tag{6.20}$$

$$f_3 = Y_3 - \alpha_{31} f_1 - \alpha_{32} f_2 \tag{6.21}$$

$$\vdots$$

$$f_n = Y_n - \sum_{j=1;n\geq 2}^{n-1} \alpha_{nj} f_j \tag{6.22}$$

where α_{nj} are constants. The next step is to obtain these constants in order to find the orthogonal function f_n. From the property of orthogonal functions (Eq. (6.1)), we can write the following relationship as

$$f_2 = Y_2 - \alpha_{21} f_1 \tag{6.23}$$

$$\int_0^1 f_2 f_1 d\eta = \int_0^1 Y_2 f_1 d\eta - \alpha_{21} \int_0^1 f_1 f_1 d\eta \tag{6.24}$$

$$0 = \int_0^1 Y_2 f_1 d\eta - \alpha_{21} \int_0^1 f_1^2 d\eta \tag{6.25}$$

$$\alpha_{2,1} = \frac{\int_0^1 Y_2 f_1 d\eta}{\int_0^1 f_1^2 d\eta} \tag{6.26}$$

As a result

$$\alpha_{i,j} = \frac{\int_0^1 Y_i f_j d\eta}{\int_0^1 f_j^2 d\eta} \tag{6.27}$$

Then, the calculation of summation constants B_n for orthogonal functions f_n,

$$\Theta = \Theta_1 + \Theta_2 \tag{6.28}$$

$$\Theta_2 = \Theta - \Theta_1 = \sum A_n Y_n \exp(-\lambda^2 \zeta) = \sum B_n f_n \exp(-\lambda^2 \zeta) \tag{6.29}$$

The boundary condition at x=0 is

$$x = 0, \qquad \Theta = 1 \tag{6.30}$$

$$\left(1 - \frac{-BrC_1^2 \rho_s^4}{4}(r^4 - 1 + 4C_2)\right) = \sum A_n Y_n = \sum B_n f_n \tag{6.31}$$

$$B_n = \frac{\int_0^1 \left(1 - \frac{-BrC_1^2 \rho_s^4}{4}(r^4 - 1 + 4C_2)\right) f_n d\eta}{\int_0^1 f_n^2 d\,\eta} \tag{6.32}$$

Then summation coefficients A_n can be found.

$$\sum B_n f_n = B_1 f_1 + B_2 f_2 + B_3 f_3 + B_4 f_4 \ldots + B_n f_n \tag{6.33}$$

$$\sum B_n f_n = B_1 Y_1 + B_2(Y_2 - \alpha_{21} f_1) + B_3(Y_3 - \alpha_{31} f_1 - \alpha_{32} f_2) + B_4(Y_4 - \alpha_{41} f_1 - \alpha_{42} f_2 - \alpha_{43} f_3) \ldots + B_n f_n \tag{6.34}$$

$$\begin{aligned}\sum B_n f_n = {} & B_1 Y_1 + B_2(Y_2 - \alpha_{21} Y_1) \\ & + B_3\big(Y_3 - \alpha_{31} Y_1 - \alpha_{32}(Y_2 - \alpha_{21} Y_1)\big) \\ & + B_4\Big(Y_4 - \alpha_{41} Y_1 - \alpha_{42}(Y_2 - \alpha_{21} Y_1) \\ & - \alpha_{43}\big(Y_3 - \alpha_{31} Y_1 - \alpha_{32}(Y_2 - \alpha_{21} Y_1)\big)\Big) \ldots + B_n f_n\end{aligned} \tag{6.35}$$

$$\begin{aligned}\sum B_n f_n = {} & Y_1(B_1 - \alpha_{21} B_2 - \alpha_{31} B_3 + \alpha_{32}\alpha_{21} B_3 - \alpha_{41} B_4 \\ & + \alpha_{42}\alpha_{21} B_4 - \alpha_{43}\alpha_{32}\alpha_{21} B_4 \ldots) \\ & + Y_2(B_2 - \alpha_{32} B_3 - \alpha_{42} B_4 + \alpha_{43}\alpha_{32} B_4 \ldots) \\ & + Y_3(B_3 - \alpha_{43} B_4 \ldots) + Y_4(B_4 \ldots) \ldots + Y_n(B_n \ldots) \\ & = \sum A_n Y_n\end{aligned} \tag{6.36}$$

$$\begin{aligned}A_1 = {} & B_1 - \alpha_{21} B_2 - \alpha_{31} B_3 + \alpha_{32}\alpha_{21} B_3 - \alpha_{41} B_4 + \alpha_{42}\alpha_{21} B_4 \\ & - \alpha_{43}\alpha_{32}\alpha_{21} B_4 \ldots\end{aligned} \tag{6.37}$$

Then by the help of software Mathematica, all summation coefficients can be obtained.

Method 2 and 3 are very similar; the only difference is, method 3 does not use an orthonormalized function.

Method 3:

Let us assume a series of orthogonal functions f_n related to our functions as,

$$f_1 = Y_1 \tag{6.38}$$

$$f_2 = Y_2 - \alpha_{21} Y_1 \tag{6.39}$$

$$f_3 = Y_3 - \alpha_{31} Y_1 - \alpha_{32} Y_2 \tag{6.40}$$

$$\vdots$$

$$f_n = Y_n - \sum_{j=1;n\geq 2}^{n-1} \alpha_{nj} Y_j \tag{6.41}$$

where α_{nj} are constants. The next step is to obtain these constants in order to find the orthogonal function f_n. From the property of orthogonal functions (Eq. (6.1)), we can write the following relationships as

$$f_2 = Y_2 - \alpha_{21} Y_1 \tag{6.42}$$

$$\int_0^1 f_2 f_1 d\eta = \int_0^1 Y_2 f_1 d\eta - \alpha_{21} \int_0^1 Y_1 f_1 d\eta \tag{6.43}$$

$$0 = \int_0^1 Y_2 f_1 d\eta - \alpha_{21} \int_0^1 Y_1 f_1 d\eta \tag{6.44}$$

$$\alpha_{21} = \frac{\int_0^1 Y_2 * f_1 d\eta}{\int_0^1 Y_1 f_1 \, d\eta} \tag{6.45}$$

$$f_3 = Y_3 - \alpha_{31}Y_1 - \alpha_{32}Y_2 \tag{6.46}$$

$$\int_0^1 f_3 f_1 d\eta = \int_0^1 Y_3 f_1 d\eta - \alpha_{31}\int_0^1 Y_1 f_1 d\eta - \alpha_{32}\int_0^1 Y_2 f_1 d\eta \tag{6.47}$$

$$0 = \int_0^1 Y_3 f_1 d\eta - \alpha_{31}\int_0^1 Y_1 f_1 d\eta - \alpha_{32}\int_0^1 Y_2 f_1 d\eta \tag{6.48}$$

Similarly

$$0 = \int_0^1 Y_3 f_2 d\eta - \alpha_{31}\int_0^1 Y_1 f_2 d\eta - \alpha_{32}\int_0^1 Y_2 f_2 d\eta \tag{6.49}$$

So, α_{31} and α_{32} can be found as

$$\begin{bmatrix} \int_0^1 Y_1 f_1 d\eta & \int_0^1 Y_2 f_1 d\eta \\ \int_0^1 Y_1 f_2 d\eta & \int_0^1 Y_2 f_2 d\eta \end{bmatrix} \begin{bmatrix} \alpha_{31} \\ \alpha_{32} \end{bmatrix} = \begin{bmatrix} \int_0^1 Y_3 f_1 d\eta \\ \int_0^1 Y_3 f_2 d\eta \end{bmatrix} \tag{6.50}$$

And finally

$$\begin{bmatrix} \int_0^1 Y_1 f_1 d\eta & \cdots & \int_0^1 Y_{i-1} f_1 d\eta \\ \vdots & \ddots & \vdots \\ \int_0^1 Y_1 f_j d\eta & \cdots & \int_0^1 Y_{i-1} f_j d\eta \end{bmatrix} \begin{bmatrix} \alpha_{i1} \\ \vdots \\ \alpha_{ij} \end{bmatrix} = \begin{bmatrix} \int_0^1 Y_i f_1 d\eta \\ \vdots \\ \int_0^1 Y_i f_j d\eta \end{bmatrix} \tag{6.51}$$

Then, the calculation of summation constants B_n for orthogonal functions f_n,

$$\Theta = \Theta_1 + \Theta_2 \tag{6.52}$$

$$\Theta_2 = \Theta - \Theta_1 = \sum A_n Y_n \exp(-\lambda^2 \zeta) = \sum B_n f_n \exp(-\lambda^2 \zeta) \tag{6.53}$$

The boundary condition at x=0 is

$$x = 0, \qquad \Theta = 1 \tag{6.54}$$

$$\left(1 - \frac{-BrC_1^2\rho_s^4}{4}(r^4 - 1 + 4C_2)\right) = \sum A_n Y_n = \sum B_n f_n \tag{6.55}$$

$$B_n = \frac{\int_0^1 \left(1 - \frac{-BrC_1^2\rho_s^4}{4}(r^4 - 1 + 4C_2)\right) f_n d\eta}{\int_0^1 f_n^2 d\,\eta} \tag{6.56}$$

Then summation coefficients A_n can be found.

$$\sum B_n f_n = B_1 f_1 + B_2 f_2 + B_3 f_3 + B_4 f_4 \ldots + B_n f_n \tag{6.57}$$

$$\begin{aligned} \sum B_n f_n = {} & B_1 Y_1 + B_2(Y_2 - \alpha_{21} Y_1) + B_3(Y_3 - \alpha_{31} Y_1 - \alpha_{32} Y_2) \\ & + B_4(Y_4 - \alpha_{41} Y_1 - \alpha_{42} Y_2 - \alpha_{43} Y_3) \ldots + B_n f_n \end{aligned} \tag{6.58}$$

$$\sum B_n f_n = Y_1(B_1 - \alpha_{21}B_2 - \alpha_{31}B_3 - \alpha_{41}B_4 \dots) + Y_2(B_2 - \alpha_{32}B_3 - \alpha_{42}B_4 \dots) + Y_3(B_3 - \alpha_{43}B_4 \dots) + Y_4(B_4 \dots) \dots + Y_n(B_n \dots) = \sum A_n Y_n \quad (6.59)$$

And finally,

$$A_n = B_n - \sum_{j=n+1}^{N} \alpha_{nj} B_j \quad (6.60)$$

Method 4:

Again similar to method 3, assume a series of orthogonal functions f_n related to our functions as,

$$f_1 = Y_1 \quad (6.61)$$

$$f_2 = Y_2 - \alpha_{21} Y_1 \quad (6.62)$$

$$f_3 = Y_3 - \alpha_{31} Y_1 - \alpha_{32} Y_2 \quad (6.63)$$

$$\vdots$$

$$f_n = Y_n - \sum_{j=1;n\geq 2}^{n-1} \alpha_{nj} Y_j \quad (6.64)$$

where α_{nj} are constants. The next step is to obtain these constants in order to find the orthogonal function f_n. From the property of orthogonal functions (Eq. (6.1)), we can write the following relationships as

$$f_2 = Y_2 - \alpha_{21} Y_1 \tag{6.65}$$

$$\int_0^1 f_2 f_1 d\eta = \int_0^1 Y_2 f_1 d\eta - \alpha_{21} \int_0^1 Y_1 f_1 d\eta \tag{6.66}$$

$$0 = \int_0^1 Y_2 Y_1 d\eta - \alpha_{21} \int_0^1 Y_1 Y_1 d\eta \tag{6.67}$$

$$\alpha_{21} = \frac{\int_0^1 Y_2 * Y_1 d\eta}{\int_0^1 Y_1^2 \, d\eta} \tag{6.68}$$

Similarly

$$f_3 = Y_3 - \alpha_{31} Y_1 - \alpha_{32} Y_2 \tag{6.69}$$

$$\int_0^1 f_3 f_1 d\eta = \int_0^1 Y_3 f_1 d\eta - \alpha_{31} \int_0^1 Y_1 f_1 d\eta - \alpha_{32} \int_0^1 Y_2 f_1 d\eta \tag{6.70}$$

$$0 = \int_0^1 Y_3 f_1 d\eta - \alpha_{31} \int_0^1 Y_1 f_1 d\eta - \alpha_{32} \int_0^1 (f_2 + \alpha_{21} Y_1) f_1 d\eta \tag{6.71}$$

$$0 = \int_0^1 Y_3 Y_1 d\eta - \alpha_{31} \int_0^1 Y_1 Y_1 d\eta - \alpha_{32} \int_0^1 f_2 f_1 d\eta - \alpha_{32}\alpha_{21} \int_0^1 Y_1 f_1 d\eta \tag{6.72}$$

$$0 = \int_0^1 Y_3 Y_1 d\eta - \alpha_{31} \int_0^1 Y_1 Y_1 d\eta - 0 - \alpha_{32}\alpha_{21} \int_0^1 Y_1 f_1 d\eta \tag{6.73}$$

Neglect the last term since $\alpha_{nj} < 1$ and $\alpha_{32}\alpha_{21} << 1$

$$\alpha_{31} = \frac{\int_0^1 Y_3 * Y_1 dr}{\int_0^1 Y_1^2 \, dr} \tag{6.74}$$

As a result, referring to [56], α_{nj}becomes,

$$\alpha_{nj} = \frac{\int_0^1 Y_n * Y_j dr}{\int_0^1 Y_j^2 \, dr} \tag{6.75}$$

Then, the calculation of summation constants B_n for orthogonal functions f_n,

$$\Theta = \Theta_1 + \Theta_2 \tag{6.76}$$

$$\Theta_2 = \Theta - \Theta_1 = \sum A_n Y_n \exp(-\lambda^2 \zeta) = \sum B_n f_n \exp(-\lambda^2 \zeta) \tag{6.77}$$

The boundary condition at x=0 is

$$x = 0, \qquad \Theta = 1 \tag{6.78}$$

$$\left(1 - \frac{-Br C_1^2 \rho_s^4}{4}(r^4 - 1 + 4C_2)\right) = \sum A_n Y_n = \sum B_n f_n \tag{6.79}$$

$$B_n = \frac{\int_0^1 \left(1 - \frac{-BrC_1^2\rho_s^4}{4}(r^4 - 1 + 4C_2)\right) f_n d\eta}{\int_0^1 f_n^2 d\,\eta} \tag{6.80}$$

Then summation coefficients A_n can be found.

$$\sum B_n f_n = B_1 f_1 + B_2 f_2 + B_3 f_3 + B_4 f_4 \ldots + B_n f_n \tag{6.81}$$

$$\begin{aligned}\sum B_n f_n = {} & B_1 Y_1 + B_2(Y_2 - \alpha_{21} Y_1) + B_3(Y_3 - \alpha_{31} Y_1 - \alpha_{32} Y_2) \\ & + B_4(Y_4 - \alpha_{41} Y_1 - \alpha_{42} Y_2 - \alpha_{43} Y_3) \ldots + B_n f_n\end{aligned} \tag{6.82}$$

$$\begin{aligned}\sum B_n f_n = {} & Y_1(B_1 - \alpha_{21} B_2 - \alpha_{31} B_3 - \alpha_{41} B_4 \ldots) \\ & + Y_2(B_2 - \alpha_{32} B_3 - \alpha_{42} B_4 \ldots) + Y_3(B_3 - \alpha_{43} B_4 \ldots) \\ & + Y_4(B_4 \ldots) \ldots + Y_n(B_n \ldots) = \sum A_n Y_n\end{aligned} \tag{6.83}$$

And finally,

$$A_n = B_n - \sum_{j=n+1}^{N} \alpha_{nj} B_j \tag{6.84}$$

DETAILED TABLES

Table 20 First 30 eigenvalues for different Pe with Kn=0, Br=0 and κ=1.667

Kn=0 Pe	**1**	**2**	**5**	**10**	**50**	**100**	**1000**	**10^6**
λ_1	1.42981	1.86754	2.3853	2.59693	2.69945	2.70313	2.70435	2.70436
λ_2	2.27757	3.12312	4.51094	5.54688	6.59595	6.65758	6.67881	6.67903
λ_3	2.88504	4.00196	5.97653	7.71385	10.3389	10.5827	10.6724	10.6734
λ_4	3.38546	4.72062	7.15791	9.45921	13.8529	14.4347	14.6686	14.6711
λ_5	3.82106	5.34393	8.17439	10.9532	17.1202	18.1898	18.6646	18.6699
λ_6	4.21193	5.90202	9.07984	12.278	20.1525	21.8322	22.6596	22.6691
λ_7	4.56954	6.41185	9.904	13.4796	22.9735	25.3531	26.6529	26.6687
λ_8	4.90115	6.88412	10.6653	14.5862	25.6099	28.7493	30.6442	30.6683
λ_9	5.21173	7.32606	11.3763	15.6171	28.0861	32.0216	34.633	34.6681
λ_{10}	5.50482	7.74285	12.0457	16.5856	30.4231	35.1738	38.619	38.6679
λ_{11}	5.78309	8.13836	12.68	17.5017	32.6386	38.2115	42.6017	42.6677
λ_{12}	6.04858	8.51553	13.2842	18.3731	34.7474	41.1411	46.5809	46.6676
λ_{13}	6.3029	8.87671	13.8621	19.2055	36.7618	43.9692	50.5561	50.6675
λ_{14}	6.54735	9.22376	14.4171	20.0039	38.692	46.7026	54.5272	54.6674
λ_{15}	6.783	9.55824	14.9515	20.7719	40.5467	49.3476	58.4937	58.6674
λ_{16}	7.01074	9.8814	15.4675	21.5128	42.3333	51.9102	62.4552	62.6673
λ_{17}	7.23131	10.1943	15.9669	22.2292	44.0582	54.3959	66.4116	66.6673
λ_{18}	7.44535	10.4979	16.4511	22.9235	45.7269	56.8098	70.3624	70.6672
λ_{19}	7.65341	10.793	16.9216	23.5975	47.3441	59.1568	74.3074	74.6672
λ_{20}	7.85596	11.0802	17.3793	24.2528	48.9139	61.4409	78.2462	78.6671
λ_{21}	8.05342	11.3602	17.8253	24.8911	50.4401	63.6663	82.1786	82.6671
λ_{22}	8.24615	11.6334	18.2604	25.5134	51.9258	65.8364	86.1043	86.6671
λ_{23}	8.43448	11.9004	18.6854	26.1211	53.374	67.9546	90.0229	90.6671
λ_{24}	8.6187	12.1615	19.101	26.7149	54.7871	70.024	93.9343	94.667
λ_{25}	8.79906	12.4171	19.5077	27.2959	56.1675	72.0472	97.8381	98.667
λ_{26}	8.9758	12.6676	19.9062	27.8649	57.5172	75.9654	101.734	102.667
λ_{27}	9.14913	12.9132	20.2968	28.4225	58.8381	79.7273	105.622	106.667
λ_{28}	9.31923	13.1542	20.68	28.9694	60.1319	83.3483	109.501	110.667
λ_{29}	9.48628	13.3909	21.0563	29.5062	61.4001	86.8418	113.372	114.667
λ_{30}	9.65044	13.6235	21.426	30.0334	62.6441	90.2192	117.235	118.667

Table 21 First 30 eigenvalues for different Pe and Kn with Br=0 and κ=1.667

Pe	1		2		5	
	Kn=0.04	**Kn=0.08**	**Kn=0.04**	**Kn=0.08**	**Kn=0.04**	**Kn=0.08**
λ_1	1.35573	1.30487	1.7741	1.70544	2.27492	2.18118
λ_2	2.17069	2.13667	2.97967	2.93118	4.31765	4.24138
λ_3	2.76906	2.76761	3.84276	3.83962	5.74721	5.73721
λ_4	3.27142	3.29696	4.56262	4.59813	6.9234	6.97604
λ_5	3.71344	3.75933	5.19423	5.25899	7.94921	8.05019
λ_6	4.11225	4.17392	5.76314	5.85049	8.86975	9.00793
λ_7	4.47809	4.55252	6.28438	6.38995	9.71081	9.87872
λ_8	4.81772	4.90288	6.76783	6.88868	10.4892	10.6818
λ_9	5.13589	5.23039	7.22042	7.35453	11.2165	11.4305
λ_{10}	5.43613	5.53893	7.64724	7.79313	11.9014	12.1342
λ_{11}	5.72108	5.83141	8.05214	8.2087	12.5504	12.8001
λ_{12}	5.99283	6.11008	8.43812	8.60448	13.1683	13.4336
λ_{13}	6.25301	6.37671	8.80756	8.98304	13.7592	14.039
λ_{14}	6.50298	6.63273	9.16239	9.34641	14.3263	14.6196
λ_{15}	6.74383	6.8793	9.50418	9.69629	14.8721	15.1783
λ_{16}	6.97648	7.11738	9.83427	10.0341	15.399	15.7172
λ_{17}	7.20171	7.3478	10.1538	10.3609	15.9086	16.2385
λ_{18}	7.42017	7.57125	10.4636	10.6778	16.4027	16.7436
λ_{19}	7.63244	7.78832	10.7646	10.9856	16.8824	17.234
λ_{20}	7.83901	7.99952	11.0575	11.285	17.349	17.711
λ_{21}	8.04032	8.20531	11.3429	11.5767	17.8035	18.1754
λ_{22}	8.23674	8.40608	11.6213	11.8613	18.2468	18.6284
λ_{23}	8.42861	8.60218	11.8933	12.1392	18.6796	19.0706
λ_{24}	8.61624	8.79392	12.1592	12.4109	19.1027	19.5029
λ_{25}	8.79988	8.98157	12.4194	12.6769	19.5167	19.9258
λ_{26}	8.97979	9.1654	12.6744	12.9373	19.9221	20.3399
λ_{27}	9.15618	9.34562	12.9243	13.1926	20.3195	20.7458
λ_{28}	9.32925	9.52243	13.1695	13.4431	20.7093	21.144
λ_{29}	9.49918	9.69603	13.4103	13.6891	21.0919	21.5347
λ_{30}	9.66614	9.86657	13.6468	13.9306	21.4678	21.9186

Table 22 First 30 eigenvalues for different Pe and Kn with Br=0 and κ=1.667

Pe	10		50	
	Kn=0.04	**Kn=0.08**	**Kn=0.04**	**Kn=0.08**
λ_1	2.48331	2.37681	2.58562	2.47199
λ_2	5.33409	5.23308	6.40113	6.27203
λ_3	7.43809	7.4146	10.0815	10.0167
λ_4	9.16213	9.22673	13.5448	13.5919
λ_5	10.6604	10.7974	16.7779	16.958
λ_6	12.0017	12.1948	19.7966	20.1102
λ_7	13.2243	13.462	22.6237	23.0597
λ_8	14.3534	14.6277	25.2812	25.8248
λ_9	15.4065	15.712	27.7885	28.4251
λ_{10}	16.3964	16.7293	30.1623	30.8795
λ_{11}	17.3328	17.6902	32.4171	33.205
λ_{12}	18.2233	18.603	34.5658	35.4163
λ_{13}	19.0738	19.4741	36.6194	37.5263
λ_{14}	19.889	20.3086	38.5876	39.5458
λ_{15}	20.6731	21.1108	40.4788	41.4842
λ_{16}	21.4291	21.884	42.3003	43.3495
λ_{17}	22.1599	22.6312	44.0583	45.1486
λ_{18}	22.8678	23.3548	45.7585	46.8875
λ_{19}	23.5548	24.0569	47.4057	48.5714
λ_{20}	24.2226	24.7393	49.0041	50.2048
λ_{21}	24.8727	25.4035	50.5575	51.7917
λ_{22}	25.5064	26.0508	52.0693	53.3356
λ_{23}	26.125	26.6826	53.5422	54.8396
λ_{24}	26.7293	27.2999	54.9792	56.3065
λ_{25}	27.3205	27.9036	56.3824	57.7387
λ_{26}	27.8992	28.4946	57.754	59.1386
λ_{27}	28.4662	29.0737	59.0961	60.5081
λ_{28}	29.0223	29.6415	60.4102	61.8489
λ_{29}	29.5679	30.1986	61.6981	63.1629
λ_{30}	30.1038	30.7457	62.9611	64.4514

Table 23 Local Nu along the entrance region for different Pe and Kn with Br=0 and κ=1.667

$\xi = \rho_s^2(2-\rho_s^2)\, x / R$	$Nu_{x,T}$					
	Pe=1		**Pe=2**		**Pe=5**	
	Kn=0.04	**Kn=0.08**	**Kn=0.04**	**Kn=0.08**	**Kn=0.04**	**Kn=0.08**
0.01	11.814	6.53153	8.47628	5.34613	4.20596	3.43716
0.02	10.3404	6.03072	6.60905	4.58696	3.57106	3.06713
0.03	9.31473	5.66296	5.62921	4.14668	3.43333	2.97999
0.04	8.54427	5.37404	5.03009	3.85853	3.39891	2.95738
0.05	7.9377	5.13778	4.63305	3.65783	3.39004	2.95139
0.06	7.44492	4.93945	4.35641	3.51259	3.38774	2.9498
0.07	7.03546	4.76985	4.15705	3.40479	3.38714	2.94938
0.08	6.68935	4.62278	4.00989	3.32334	3.38699	2.94926
0.09	6.39285	4.49387	3.89936	3.261	3.38695	2.94923
0.1	6.13604	4.37987	3.81526	3.21285	3.38693	2.94922
0.2	4.71987	3.70429	3.5451	3.05292	3.38693	2.94922
0.3	4.16477	3.41181	3.51961	3.03717	3.38693	2.94922
0.4	3.9016	3.2658	3.51705	3.03555	3.38693	2.94922
0.5	3.76605	3.18837	3.5168	3.03539	3.38693	2.94922
0.6	3.6933	3.14607	3.51677	3.03537	3.38693	2.94922
0.7	3.6534	3.12261	3.51677	3.03537	3.38693	2.94922
0.8	3.63126	3.1095	3.51677	3.03537	3.38693	2.94922
0.9	3.61889	3.10214	3.51677	3.03537	3.38693	2.94922
1.0	3.61196	3.098	3.51677	3.03537	3.38693	2.94922
2.0	3.6031	3.09267	3.51677	3.03537	3.38693	2.94922
3.0	3.60307	3.09265	3.51677	3.03537	3.38693	2.94922
4.0	3.60307	3.09265	3.51677	3.03537	3.38693	2.94922

Table 24 Local Nu along the entrance region for different Pe and Kn with Br=0 and κ=1.667

$\xi = \rho_s^2(2-\rho_s^2)\, x / R$	$Nu_{x,T}$			
	Pe=10		**Pe=50**	
	Kn=0.04	**Kn=0.08**	**Kn=0.04**	**Kn=0.08**
0.01	3.35259	2.92826	3.29322	2.88748
0.02	3.32543	2.90867	3.29322	2.88748
0.03	3.32512	2.90842	3.29322	2.88748
0.04	3.32512	2.90842	3.29322	2.88748
0.05	3.32512	2.90842	3.29322	2.88748
0.06	3.32512	2.90842	3.29322	2.88748
0.07	3.32512	2.90842	3.29322	2.88748
0.08	3.32512	2.90842	3.29322	2.88748
0.09	3.32512	2.90842	3.29322	2.88748
0.1	3.32512	2.90842	3.29322	2.88748
0.2	3.32512	2.90842	3.29322	2.88748
0.3	3.32512	2.90842	3.29322	2.88748
0.4	3.32512	2.90842	3.29322	2.88748
0.5	3.32512	2.90842	3.29322	2.88748
0.6	3.32512	2.90842	3.29322	2.88748
0.7	3.32512	2.90842	3.29322	2.88748
0.8	3.32512	2.90842	3.29322	2.88748
0.9	3.32512	2.90842	3.29322	2.88748
1.0	3.32512	2.90842	3.29322	2.88748
2.0	3.32512	2.90842	3.29322	2.88748
3.0	3.32512	2.90842	3.29322	2.88748
4.0	3.32512	2.90842	3.29322	2.88748